A STUDY OF THE GLOBULAR CLUSTER M3

Thesis by

Allan R. Sandage

In Partial Fulfillment of the Requirements

for the Degree of

Doctor of Philosophy

California Institute of Technology

Pasadena, California

April, 1953

ACKNOWLEDGEMENTS.

I wish to express my gratitude, which all students of astronomy at this institute must feel who work on observational problems, to the Observatory Council of the Mount Wilson and Palomar Observatories for the privilege of using the equipment on Mount Wilson to secure the necessary observations.

Many thanks are due to the entire staff of the Department of Astronomy at the California Institute of Technology and the staff of the Mount Wilson and Palomar Observatories for the many kindnesses shown me during the past four years.

It is a special pleasure to express my gratitude to Dr. Walter Baade for his constant enthusiasm, personal inspiration and material help given freely during this investigation.

Discussions with Dr. Martin Schwarzschild and Dr. Fred Hoyle, especially concerning the topics of chapter 3, have been illuminating and are gratefully acknowledged.

Many thanks are due to Dr. Edwin Hubble whose suggestions on the form of the presentation have been helpful.

Mr. W. C. Miller and Mr. Harold Kinney have been helpful in preparing the illustrations.

ABSTRACT

The color-magnitude diagram for the globular cluster M3 has been obtained to absolute magnitude $M_V = +6$. The main sequence has been found, extending from $M_V = +3.5$ to the limit of the data. The photometric parallax of m - M = 15.63 is found by fitting the apparent magnitude diagram to O. J Eggen's and H. L. Johnson's diagram for stars in the solar neighborhood. The absolute magnitude of the cluster type variables in M3 is calibrated by this method. The value $M_V = 0.0$ for these stars is correct within $0^m.15$. This value is of significance for a decision on a new distance scale for the extragalactic nebulae in the observable universe.

The luminosity function is obtained to $M_V = 6.8$ for M3. From $M_{Bol} = +2$ to $+4$ a linear relation between log $\varphi(M)$ and M_{Bol} exists. The results of Chapter 3 show that this relation is expected if the sequences of the color-magnitude diagram are evolutionary in origin.

Application of a theory of evolution to the color magnitude diagram gives an age of 5×10^9 years since the formation of the main sequence in M3 and M92.

Further consequences of an evolutionary interpretation of the data are discussed in Chapter 3 and it is concluded that all evidence now available lends support to the evolutionary explanation of the sequences in the color-magnitude diagram.

Table of Contents

Table of Contents

INTRODUCTION AND SUMMARY.

The epoch of modern research on globular clusters can be traced to Solon I. Bailey's announcement[1] in 1898 of large numbers of variable stars in the clusters Messier 3 and Messier 5. Although globular clusters had been known since Ihle's initial discovery in 1665 of the cluster now known as M22, Halley's discovery of ω Centauri in 1677, Kirch's discovery of M5 in 1702 and the discovery in 1714, again by Halley, of M13, no significant research on these objects was possible until the era of large telescopes and the photographic process. Bailey's work laid the foundation for the first reliable determination of the distances to these objects by Harlow Shapley working with the 60-inch telescope on Mount Wilson in the 1920's. Shapley's early work not only changed the concept of the sun's position in our Milky Way system by placing it at the extreme edge of our galaxy but also showed that the individual characteristics of globular clusters were of unique interest. In particular, the color-magnitude diagrams for globular clusters were completely different from the diagrams for galactic clusters and for stars in the solar neighborhood. This fact was among the data which permitted Baade in 1944 to separate the two stellar population types.

Shapley's work was carried to the limit of the existing photometric scales, optical equipment and photographic materials available at that time. The brighter portions of his diagram clearly showed the importance of extending the study to fainter stars but developments lowering the limits for the detection of light were not forthcoming and the subject of the color-magnitude diagrams for globular clusters remained at the status quo. A few studies in the 1930's and early 40's of the bright stars in additional clusters were made by Cuffey, Greenstein, and Hachenberg, but no attempt was made to reach faint magnitudes.

Interest in the subject has been revived recently by two developments. (1) Baade's recognition of the two population types[2] has stimulated a search for differences in selected aggregates of pure populations I and II. (2) Technical advances in the fields of photographic emulsions, electronics, and optical instrumentation have pushed the limit of detection to fainter apparent magnitudes.

It was early realized that the 200-inch Hale telescope, using the fast photographic emulsions now available, would reach absolute magnitude +6 in some of the nearby northern clusters. Not only would the faint ends of the color-magnitude diagrams for such clusters be of intrinsic interest but they further promised to provide one step in a re-determination of the cosmic

distance scale now open to revision.[3,4,5] Furthermore, detailed studies of the luminosity function and radial density distribution within a typical globular cluster could be pushed significantly farther than was possible with the equipment of the 1920's. Consequently, the present work on the globular cluster M3 was undertaken.

This thesis reports the results of a study of (a) the color-magnitude diagram, (b) the luminosity function to $M_V = +7$, and (c) the projected radial density distribution $\rho(m_{pv}, r)$ for the globular cluster M3. Both the 100-inch and 200-inch telescopes were used to obtain the observational data. These data suggest an evolutionary theory for stars which do not internally mix. This theory appears to explain most of the observed facts presented in Chapter 1 and 2 of this thesis. A brief summary of the observational results follows.

The color-magnitude diagram for M3 has been obtained from $m_{pv} = 12.6$ to $m_{pv} = 21.2$. All known variable stars were excluded from those photometered. The diagram shows a well defined giant sequence, a horizontal sequence situated in the Hertzsprung-Russell gap, a transition and subgiant sequence and finally a heavily populated globular cluster main sequence. Slightly more than two magnitudes of the main sequence has been obtained. There is a distinct gap containing the cluster type

variables in the horizontal sequence. This gap occurs at $m_{pv} = 15.63$. If $M_V = 0.0$ is adopted for these variable stars, the distance modulus for M3 is $m - M = 15.63$. The presence of this gap strongly emphasizes the supposition that a star, to become a cluster variable, must pass into a well-defined state characterized by definite values of its absolute luminosity, chemical composition and radius.

A comparison of the color-magnitude diagram of M3 with that of M92, obtained by Arp, Baum and the present author[6], shows significant differences, the most striking of which is the color shift of the giant, transition, subgiant, and main sequences. This may be explained by a chemical composition difference in the stars of the two clusters. The difference can quantitatively be explained if the stars in M3 have 1.3 times the metal abundance of stars in M92.

An absolute magnitude calibration of the cluster type variables in M3 is possible in principle by fitting the M3 sequencesto similar sequences of stars in the solar neighborhood. The question of the proper identification of the cluster main sequence arises and discussion shows that this calibration can be made without exact knowledge of the nature of the globular cluster main sequence. It turns out that precise identification of globular cluster main sequence with dwarfs or subdwarfs

unimportant if the color-magnitude diagram for stars in the solar neighborhood is similar to that given by Olin Eggen[7]. The data indicate that the value $M_v = 0.0$ for the variables, obtained by this matching, is a good one. An evolutionary theory for unmixed stars, given in Chapter 3, applied to the color-magnitude diagram gives a time of 5×10^9 years since all stars were on the main sequence of M3 and M92. This may be taken as the age of these globular clusters.

The total luminosity function, $\varphi(M)$ for M3 has been obtained from $M_{pv} = -3.0$ to $M_{pv} = +6.8$ by star counts on plates exposed to reach different limiting magnitudes. The stars along the horizontal sequence provide the well known hump in $\varphi(M)$ at $M_{pv} = 0.0$. To $M_{pv} = +7.0$ there are 46,000 stars in M3. If Van Rhijn's[8] luminosity function applies for M_v fainter than $M_{pv} = 7$, there are a total of 280,000 stars in M3 from $M_{pv} = -3$ to +18. There is, however, no compelling reason why Van Rhijn's $\varphi(M)$ which is valid in the solar neighborhood, should apply to the globular cluster main sequence. If Van Rhijn's $\varphi(M)$ did apply and if the mass-luminosity relation is valid in M3 fainter than $M_{pv} = +4$, the total mass of M3 would be 1.1×10^5 M ⊙. This is a factor of five smaller than O. C. Wilson's preliminary dynamical value of 5.6×10^5 M ⊙ for M92 - a similar cluster. This discrepancy indeed points to the non-validity of Van Rhijn's $\varphi(M)$ in globular

clusters indicating that dwarfs stars are more numerous by a factor of about 10 in a globular cluster population compared with population I systems.

The total apparent magnitude of M3 obtained by integration of $\varphi(M)$ weighted by the proper intensity factors is $m_{pg} = 7.52$. This is in good agreement with Christie's measured value[9] of $m_{pg} = 7.21$ and gives confidence that the $\varphi(M)$ obtained in this study is essentially correct.

A knowledge of $\varphi(M)$ is important since this function presumably represents either a cosmogonic or an evolutionary property of the stellar system. If it is cosmogonic, it reflects the initial conditions of star formation. If it is evolutionary it gives the rate at which stars are moving through a given luminosity range. Simple arguments presented in Chapter 3 indicate that the shape of $\varphi(M)$ from $M_{Bol} = +1$ to $+4$ is very close to that predicted on the picture of evolution there presented. The evidence available indicates that the unique globular cluster sequences of the color-magnitude diagram do indeed find their explanation in evolutionary processes.

Chapter 1. The Color-Magnitude Diagram for M3

1.1 Introduction

The Hertzsprung-Russell diagram or its close equivalent, the color-magnitude diagram, has become an important summarizing plot in which many of the properties of stars are either implicitly or explicitly given. The great usefulness of this diagram in presenting the systematic astrophysical features of the members of a stellar aggregate demands that the greatest possible precision be attained in determining its data. The importance of a detailed study of a typical globular cluster to the magnitude limit of the 200-inch lies in (1) the possibility of finding the shape of the unique type II sequences in a color-magnitude diagram and (2) calibrating the absolute magnitude of the RR Lyrae stars by a method independent of statistical parallax studies. The study of the globular cluster M3 was undertaken with the 100-inch and 200-inch telescopes in the Spring of 1951. The final observational material was obtained in February, 1953.

To obtain the precision required, a combination of photographic and photoelectric techniques was used. The photoelectric calibration of a two color primary standard sequence far out from the cluster nucleus made it possible, through photographic procedures, to obtain a secondary standard sequence near the cluster center. This secondary sequence provided the standards for the

measurements of more than 1000 additional cluster stars. The magnitude system and measuring technique are described in the next two sections of this chapter while the resulting data in terms of the color-magnitude diagram are discussed in the last two sections.

1.2 The Magnitude Standards

Eighteen stars in the vicinity of M3 were measured photoelectrically by W. A. Baum and the author on April 11 and 12, 1951, at the 100-inch telescope. These stars, ranging in magnitude from P = $10^{m}.95$ to $19^{m}.27$, formed the primary magnitude standards upon which all the subsequent photometry was based. The photoelectric equipment had as its detector an EMI 5060 end-on phototube behind Schott BGI + GGI filters for the blue response and a Schott GG7 filter for the yellow response. The zero points for the blue and yellow magnitude scales were obtained from five photoelectric intercomparisons with Selected Area 57. Transformation to the P and V magnitude system of Stebbins, Whitford, and Johnson[10] was made from measurements of stars 29, 52, 54, and 57 in Selected Area 57. Four stars do not give sufficient data to define well a color transformation. The bluest of these four stars is number 57 with P - V = $+0^{m}.46$ while the reddest is number 52 with P - V = $+1^{m}.18$. The color transformation to the P,V system is well defined in this range, but for stars bluer than P - V = $+0^{m}.46$ a

linear extrapolation of the color equation was adopted. However, subsequent photoelectric measures by Baum[11] confirm the color equation (to P - V = 0.0) and the magnitude system first adopted for these eighteen stars. The adopted values are given in Table 1; n is the number of observations and r is the radial distance from the cluster center. Von Zeipel's numbers[12] are used for all but the three faintest stars: for these the letters a, b and c are assigned. The 18 photoelectric stars are identified on Figure 5. I am indebted to Mr. Baum for his aid and interest in the measurements for this initial sequence at an early stage of this work.

The majority of the 18 primary photoelectric standards are more distant than 8 minutes of arc from the cluster center. Large field corrections for these stars were to be expected on plates taken with the 200-inch Hale telescope since the radius of the corrected field for the Ross f/3.67 corrector lens is only slightly greater than 8 minutes. To avoid these field corrections for the 200-inch a secondary sequence of sixty-four stars was set up closer to the cluster nucleus than the primary standards. Plates taken with the 100-inch telescope, diaphragmed to 58 inches, were used to determine their magnitudes since the 100-inch so diaphragmed has a field large enough (radius of 10 minutes of arc) to include most of the photoelectric standards. Magnitudes in two colors for these sixty-four

Table 1+

The Photoelectric Standard Sequence

Star *	P	V	n	r'
206	10.95	9.86	1	7.5
1402	13.15	12.67	8	9.8
1397	14.28	12.70	2	7.5
297	14.25	12.86	3	7.5
237	14.58	14.07	1	6.7
216	15.00	14.15	1	9.2
153	15.11	14.24	5	13.0
179	15.24	14.71	2	7.9
155	15.40	14.60	1	10.1
193	15.46	14.74	1	9.7
235	15.72	15.72	2	7.7
182	15.73	15.73	1	10.5
167	15.83	15.17	1	8.7
1331	15.95	15.27	1	9.5
180	16.20	15.19	1	9.6
a	17.49	16.77	2	10.0
b	18.58	17.90	2	9.4
c	19.27	19.12	2	9.0

* Von Zeipels' numbers.[12]

\+ Stars are identified in Figure 5.

stars were determined from the 100-inch plates with the iris photometer[13] at the California Institute of Technology by interpolation between the eighteen photoelectric standards. Nine Eastman 103a0 plates taken behind a Schott WG2 filter† were photometered for the blue magnitudes and nine Eastman 103aD plates taken behind a Schott GG11 filter provided the yellow magnitudes of the 64 secondary sequence stars. The procedure for obtaining magnitudes and colors on the system of the photographic plate and filter combinations was that described in the paper[6] on M92.* The adopted m_{pg} and m_{pv} values for these sixty-four stars are given in Table 2. The stars are identified on Figure 5.

Fainter than V = $19^m.12$, P = $19^m.27$, no photoelectric calibration exists. This, therefore, is the faintest limit which is fully calibrated in the sixty-four star secondary sequence. A sequence of twenty-three additional standards, all fainter than the photoelectric limit, was calibrated provisionally by extrapolation of the magnitude scales

---

* The notation in this thesis for magnitudes on the color system of the plate and filter combinations (103a0 + WG2; 103aD + GG11) is m_{pg} and m_{pv}. These are quantities identical with P' and V' in the paper on M92[5]. The color index on the system of the photographic materials is denoted in this paper by CI = $m_{pg} = m_{pv}$ instead of P' - V' as in reference 6.

† The Schott WG2 filter together with an aluminized mirror has nearly the same ultra-violet transmission characteristics as a silvered mirror. The blue magnitudes derived with this plate, filter, and mirror combination are therefore nearly on the international photographic system as originally defined.

Table 2

Sixty-Four Stars of the Secondary Sequence*

Star	m_{pg}	m_{pv}	SD Letter	Star	m_{pg}	m_{pv}	SD Letter
A	14.51	13.31	SD c	AG	16.51	15.85	
B	14.10	13.60	SD a	AH	14.80	13.79	
C	15.55	15.57		AI	16.79	16.14	
D	15.83	15.06		AJ	16.94	16.33	
E	17.13	16.44		AK	17.83	17.18	
F	18.62	17.91		AL	19.07	18.77	
G	16.84	16.16		AM	15.35	14.99	
H	15.64	14.93		AN	15.76	15.93	SD k
I	18.56	18.26		AO	15.35	14.71	
J	19.55	19.28		AP	18.86	18.26	
K	18.01	17.90		AQ	15.99	15.69	SD m
L	15.85	15.09		AR	15.86	15.58	SD l
M	16.72	16.02		AS	18.99	18.52	
N	17.44	16.84		AT	16.27	15.59	SD n
O	17.34	16.78		AU	16.45	15.82	
P	17.04	16.33		AV	15.00	14.12	
Q	18.40	17.64		AW	15.47	14.81	
R	17.21	16.75		AX	15.55	15.56	
S	15.00	14.10	SD e	AY	17.24	16.56	SD p
T	15.27	14.60	SD f	AZ	16.62	15.96	SD o
U	14.60	13.57	SD d	BA	18.54	17.86	
V	15.47	14.86	SD g	BB	15.48	14.71	
W	16.56	15.60		BC	14.92	13.97	
X	17.48	16.78		BD	19.05	18.32	
Y	17.05	16.38		BE	15.37	14.66	
Z	15.66	15.78	SD h	BF	14.74	13.75	
AA	14.23	12.70	SD b	BG	15.10	14.29	
AB	17.13	16.42		BH	15.32	14.63	
AC	15.61	14.83		BI	15.01	14.11	
AD	17.89	17.23		BJ	16.12	15.42	
AE	14.77	13.94		BK	17.52	16.84	
AF	15.61	15.68		BL	16.13	15.40	

* Identified on Figure 5.

to $m_{pv} = 21^{m}.2$, $m_{pg} = 21^{m}.8$ by extending the iris photometer calibration curves for three long exposure plates in each color beyond $V = 19^{m}.12$, $P = 19^{m}.27$. Since the characteristic curves for the instrument in this image density range are well known, the extrapolation can be made with some confidence. Furthermore, one photographic intercomparison with SA 57 was in good agreement with the extrapolated m_{pg} values. The magnitude sources for this thesis are then, (1) a primary photoelectric sequence of 18 stars and (2) a secondary photographic sequence of 87 stars. The total magnitude range covered by these stars is from $m_{pv} = 12^{m}.7$, $m_{pg} = 13^{m}.1$ to $m_{pv} = 21^{m}.2$, $m_{pg} = 21^{m}.8$.

Included in the 87 standard stars are the 14 standards of Shapley and Davis[14] upon which they based their early work on M3. A comparison of their magnitudes with the values derived in this investigation is shown in Table 3.

1.3 The Photographic Measurements

Photographic and photovisual magnitudes of more than 1000 stars were determined by interpolation between the 87 secondary standards from 21 plates taken with the 100-inch and 200-inch telescopes. Three series of plates were measured with the iris photometer to cover the entire magnitude interval from $m_{pv} = 12^{m}.7$ to $21^{m}.2$. Data for the plates of each series are given in Table 4. All plates with the 200-inch Hale telescope were taken

Table 3

Comparison with Shapley and Davis' Magnitudes

Star*	Shapley and Davis		Present Investigation	
	m_{pg}	m_{pv}	m_{pg}	m_{pv}
a	14.04	13.34	14.10	13.60
b	14.05	12.26	14.23	12.70
c	14.57	13.39	14.51	13.31
d	14.53	13.41	14.60	13.57
e	14.81	13.91	15.00	14.10
f	15.06	14.53	15.27	14.60
g	15.22	14.57	15.47	14.86
h	15.53	15.55	15.66	15.78
k	15.63	15.67	15.76	15.93
l	15.83	15.50	15.86	15.58
m	15.94	15.25	15.99	15.69
n	16.16	15.48	16.27	15.59
o	16.37	15.72	16.62	15.96
p	16.84	16.43	17.24	16.56

*Notation of Shapley and Davis

Table 4
List of M3 Plates

Plate No.	Date	Plate and Filter	Exposure Time Min.	Telescope	
		Series I Magnitude Range $12^m.7$ - $17^m.5$			
H 76 S	March 7, 1951	103aO + WG2	10	100-inch	+
H 80 S	March 7, 1951	103aO + WG2	5	100-inch	+
H 107 S	May 4, 1951	103aO + WG2	7	100-inch	+
H 68 S	March 6, 1951	103aD + GG11	20	100-inch	+
H 75 S	March 7, 1951	103aD + GG11	15	100-inch	+
H 102 S	May 3, 1951	103aD + GG11	15	100-inch	+
		Series II Magnitude Range $17^m.0$ - $19^m.2$			
H 86 S	April 10, 1951	103aO + WG2	15	100-inch	+
H 97 S	May 3, 1951	103aO + WG2	30	100-inch	+
H 90 S	May 2, 1951	103aO + WG2	20	100-inch	+
H 110 S	May 4, 1951	103aD + GG11	60	100-inch	+
H 119 S	June 7, 1951	103aD + GG11	40	100-inch	∓
PH 611 B	May 14, 1952	IIaO + GG1	10	200-inch	*
PH 612 B	May 14, 1952	IIaO + GG1	10	200-inch	*
PH 613 B	May 14, 1952	103aD + GG11	10	200-inch	*
PH 615 B	May 14, 1952	103aD + GG11	10	200-inch	*
		Series III Magnitude Range $18^m.8$ - $21^m.2$			
PH 377 B	June 1, 1951	103aO + GG1	25	200-inch	*
PH 378 B	June 1, 1951	IIaO + GG1	25	200-inch	*
PH 392 B	June 3, 1951	IIaO + GG1	25	200-inch	*
PH 379 B	June 1, 1951	103aD + GG11	65	200-inch	*
PH 393 B	June 3, 1951	103aD + GG11	50	200-inch	*
PH 394 B	June 3, 1951	103aD + GG11	50	200-inch	*

+ diaphramed to 58 inches. ∓ with the Ross zero corrector lens. *With the Ross f/3.67 corrector lens. Taken by Baade.

by Dr. W. Baade. I am grateful to Dr. Baade for the privilege of using these plates. His material aid in the problem has made a large portion of this study possible.

Stars in the magnitude range covered by series I plates (all with the 100-inch) were selected for measurement from an annulus whose inside radius was 100 seconds of arc and whose outside radius was 600 seconds. Stars in the magnitude interval covered by series II plates (100-inch and 200-inch) were selected from an annulus whose inside radius was 200 seconds and whose outside radius was 500 seconds. This outer radius of 500 seconds is just within the correction-free field of the 200-inch. Stars in the magnitude interval covered by series III plates (all with the 200-inch) were selected for measurement from a sixty degree sector of a ring whose inner boundary was a circular arc of 200 seconds radius and whose outer boundary was a circular arc of 400 seconds radius. All known variable stars[15] and all stars crowded by close companions were excluded from the photometry. The final m_{pg} and m_{pv} values adopted for any star are the means from all values determined from the plates of Table 4. Three independent blue, and three independent yellow measures for stars of series I and III were available, while the values for stars of series II rest solely upon the 200-inch material for which two measures in each color

were available. The estimated probable errors of the final magnitudes and colors, judged from the internal consistency of the measures, are

$$\varepsilon(m_{pg}) = \pm 0^{m}.015$$
$$\varepsilon(m_{pv}) = \pm 0^{m}.014 \qquad 12^{m}.7 < m_{pv} < 17^{m}.5$$
$$\varepsilon(CI) = \pm 0^{m}.022$$

$$\varepsilon(m_{pg}) = \pm 0^{m}.016$$
$$\varepsilon(m_{pv}) = \pm 0^{m}.013 \qquad 17.0 < m_{pv} < 19.2$$
$$\varepsilon(CI) = \pm 0^{m}.021$$

$$\varepsilon(m_{pg}) = \pm 0^{m}.014$$
$$\varepsilon(m_{pv}) = \pm 0^{m}.016 \qquad 18.8 < m_{pv} < 21.2$$
$$\varepsilon(CI) = \pm 0^{m}.021$$

The overlap of the 100-inch and 200-inch material in the series II magnitude interval permitted an evaluation of the color equation differences between the two telescopes. A residual color difference of $0^{m}.03$ was detected and all 200-inch data were reduced to the m_{pg}, m_{pv} system of the 100-inch by applying this correction. The relation between the 100-inch m_{pg}, m_{pv} system and the P, V system of Stebbins, Whitford and Johnson[10] was determined from measurements of plates of Selected Area 57 and 61. The color equations adopted

are

$$P - V = 0.92\ (CI) + .05 \qquad (1)$$

$$P = m_{pg} - 0.09\ (P-V) + .05 \qquad (2)$$

$$V = m_{pv} \qquad (3)$$

where $CI = m_{pg} - m_{pv}$ (4)

Due to additional data, these differ slightly from the equations in the paper[6] on M92. Table 6 gives the adopted m_{pv} and CI values for all measured stars. This table is arranged in three sections, one section for each of the three magnitude series. The star numbers refer to stars identified on Figure 6, 7 and 8. There is no correspondence of this numbering system with Von Zeipel's.[12] For magnitude series I and II (stars identified on Figures 6 and 7) the cluster has been divided into six sectors for ease of numbering. The designation of a star is given in Roman numerals by the sector in which it is located and by its number within that sector; e.g. Series II, Sector IV, 56. Series III ($18.8 < m_{pv} < 21.2$) stars are located on figure 8 which is divided into two sections. The stars are designated in Table 6 by the section (I or II) together with the number within the section, e.g. I, 210.

1.4 The Color-Magnitude Diagram

The color-magnitude diagram from these data is shown in Figure 1. This diagram does not represent

TABLE 6

MAGNITUDES AND COLORS OF 1043 STARS IN M 3

Series I $12.7 < m_{pv} < 18.0$

No.	m_{pv}	CI	No.	m_{pv}	CI	No.	m_{pv}	CI	No.	m_{pv}	CI	No.	m_{pv}	CI	No.	m_{pv}	CI
I, 1	15.18	0.60	II, 1	16.01	.40	III,44	14.35	0.80	IV, 59	15 17	0.67	V, 58	17.17	0.66	VI,74	15.39	-0.07
2	15.10	0.72	2	16.76	0 57	45	1.45	0.64	60	15.56	0.26	59	16.84	0.59	75	15.56	0.27
3	17.56	0.59	3	15.27	0.71	47	16.40	0.65	61	16.21	0.62	60	15.43	0.68	76	14.07	0.90
4	16.85	0.55	4	15.97	-0.21	49	17.24	0.65	63	15.85	-0.20	61	15.71	-0.12	77	16.58	0.58
5	16.34	0.70	5	16.04	0.66	50	17.01	0.59	64	15.51	0.67	62	17.35	0.13	78	15.47	0.39
I, 7	15.61	-0.09	II, 6	15.61	-0.14	III,51	15.60	0.1,	IV, 65	16.62	0.59	V, 64	17.05	0.62	VI,79	15.11	0.79
8	16.03	0.45	7	15.53	0.61	52	16.70	0.68	66	15.07	0.67	65	16.48	0.67	80	14.46	0.90
9	16.44	0.56	8	15.74	-0.11	53	15.38	0.60	67	15.86	-0.22	66	16.79	0.64	81	15.45	0.30
11	16.55	0.64	9	16.84	0.60	54	17.29	0.67	68	14.77	0.58	67	17.24	0.65	82	14.58	0.85
13	17.01	0.53	10	17.32	0.56	5,	14.63	0.75	69	15.95	0.66	68	14.78	0.57	83	15.80	0.72
I, 14	15.74	0.66	II, 11	15.70	0.18	III,56	14.71	0.56	IV, 70	17.06	0.62	V, 69	15.64	0.66	VI,84	15.35	0.39
15	14.65	0.86	12	15.09	0.58	57	16.69	-0.41	71	14.84	0.70	70	15.53	0.71	85	15.47	-0.05
17	15.58	0.71	13	15.72	-0.11	58	16.01	0.66	72	16.01	.61	71	15.41	0.66	86	14.71	0.68
19	15.02	0.77	14	17.45	0.64	59	16.91	0.66	73	16.10	0.61	72	15.67	0.59			
21	13.05	1.31	15	15.62	0.24	60	16.41	0.64	74	15.15	0.64	73	15.43	0.31			
															Series II		
															$17.0 < m_{pv} < 19.2$		
I, 27	15.99	-0.25	II 16	14.18	0.10	III,61	16.29	0.5	IV, 75	15.68	-0.16	V, 74	15.39	0.64	I, 1	18.56	0.15
29	15.03	0.73	21	14.39	0.06	62	17.12	0.37	76	15.45	0.58	75	15.65	-0.07	2	19.11	0.45
30	15.80	-0.17	22	16.53	0.70	63	14.31	0.67	77	13.27	1.13	76	16.16	0.69	3	18.77	0.48
31	17.26	0.69	24	16 99	0.65	64	13.16	1.21	78	15.89	-0.19	77	14.62	0.80	4	19.30	0.50
32	17.34	0.70	26	16.87	0.60	65	15.10	-0.10	79	16.07	-0 27	78	14.35	0.78	5	17.58	0.69
I, 34	14.70	0.78	II, 28	16.66	0.65	III,66	16.04	0.66	IV, 80	14.34	0.79	V, 79	16.16	-0 26	I, 6	18.48	0.69
36	16.06	0.62	32	15.88	0.74	67	15.21	0.66	81	15.44	0.69	80	13.50	0.99	7	19.06	0.46
38	16.41	0.67	33	15.74	-0.11	68	16.05	0.65	82	13.51	1.26	81	15.96	-0.17	8	18.65	0.50
39	14.48	0.82	34	17.02	0.62	69	14.70	0.73	84	15.80	0.64	82	15.63	-0.13	9	18.77	0.46
40	15.64	0.26	35	16.34	0.65	70	14.61	0.59	85	14.55	0.79	83	15.75	-0.16	10	18.71	0.46
I, 41	16.60	0.63	II, 36	17.18	0.65	III,71	14.95	0.70	IV, 86	15.63	-0.05	V, 84	15.15	0.68	I, 11	19.02	0.42
42	15.58	0.22	37	17.0	0.65	72	15.48	0.03	87	15.89	0.25				12	19.28	0.52
43	16.70	0.72	38	16.88	0.61	73	14.96	0.69	88	15.35	0.66				14	19.27	0.45
44	16.34	0.68	39	16.76	0.61	74	14.95	0.50	89	14.38	0.76				19	17.27	0.68
46	13.89	1.00	40	17.01	0.63	75	15.59	0.30	90	15.65	-0.1,				20	18.92	0.40
I, 47	16.26	-0.26	II, 42	14.80	0.56	III,76	15.78	0.65	IV, 91	15.38	0.31	VI, 1	15.50	0.44	I, 22	17.51	0.68
48	16.87	0.74	43	13.76	0.66	77	13.96	1.15	92	15.65	-0.05	2	16.30	0.61	23	18.40	0.62
49	11.13	0.67	44	15.65	0.66	78	15.79	0.68	94	15.55	0.61	3	17.21	0.31	24	19.22	0.43
50	17.58	0.74	45	15.65	-0.05	79	15.72	-0.14	95	14.74	0.71	4	16.91	0.63	25	19.23	0.38
51	11.73	-0.02	46	12.72	1.48	80	13.26	1.06	98	15.64	0.20	5	17.53	0.81	26	19.19	0.42
I, 52	15.39	0.70	II, 47	15.61	0.32	III,81	14.63	0.70	IV, 99	16.64	0.57	VI, 6	16.22	0.70	I, 27	18.54	0.52
53	17.28	0.71	48	16.02	0.70	82	15.41	0.63	100	15.55	0.34	7	17.37	0.71	28	18.54	0.55
54	16.60	0.59	50	16.91	0.64	83	15.75	-0.1,	101	13.53	1.20	8	14.34	0.70	29	19.42	0.38
55	13.52	0.55	51	17.44	0.61	84	15.14	0.64	102	15.56	-0.13	9	16.00	1.45	30	18.57	0.49
56	16.26	-0.26	52	16.19	0.66	85	16.4,	0.11				14	15.59	0.68	32	18.96	0.40
I, 5,	16.99	0.73	II, 53	15.67	0.29	III,86	16.28	0.2	V, 1	**16.92**	0.64	VI,16	16.30	0.81	I, 33	18.90	0.38
58	17.10	-0.5,	54	15.16	0.66	87	17.73	-0.77	2	16.62	0.67	17	16.54	0.73	34	18.86	0.39
5,	17.55	0.65	56	16.96	0.73				3	15.45	0.70	18	15.71	-0.02	35	18.51	0.49
6,	13.50	0.61	57	15.05	-0.71				4	17.07	0.96	21	15.88	0.65	36	19.60	0.42
62	15.65	0.30	58	16.68	0.65				5	16.07	**0.69**	22	15.88	0.65	37	18.95	0.42
I, 63	12.43	0.69	II, 59	11.02	0.80	IV, 1	15.83	0.49	V, 6	17.43	0.18	VI,23	16.14	0.69	I, 38	18.38	0.61
64	16.42	0.74	61	14.19	0.94	2	16.24	0.71	7	15.41	0.71	24	16.69	0.68	39	19.33	0.34
65	13.54	0.31	62	14.39	0.77	3	14.18	0.86	8	16.74	0.76	25	16.34	0.69	40	18.91	0.43
66	16.29	0.63	63	15.72	-0.07	4	16.31	0.64	9	**17.05**	0.68	26	15.74	-0.11	43	17.93	0.60
67	15.24	0.71	64	14.83	0.73	7	17.08	0.71	11	16.84	0.69	28	16.87	0.72	44	17.09	0.63
I, 69	15.97	0.66	II, 6,	15.54	0.32	IV, 7	15.54	0.43	V, 12	15.16	0.65	**VI**,29	15.66	0.25	I, 45	19.17	0.32
70	17.04	0.64	66	15.97	-0.34	8	16.68	0.61	13	15.08	1.07	30	15.62	0.72	46	19.47	0.32
71	15.41	0.33	67	16.13	-0.26	15	15.77	0.60	14	15.65	**0.73**	31	15.21	0.69	47	17.90	0.58
72	14.63	0.81	68	14.21	0.85	17	15.34	0.69	15	**15.76**	0.68	34	15.71	-0.09	48	19.23	0.36
73	17.36	0.69				18	15.95	-0.23	16	**15.77**	-0.12	36	17.50	0.83	49	19.25	0.44
I, 75	14.81	0.73	III, 1	16.29	0.68	IV, 19	15.82	0.64	V, 17	**15.54**	0.27	VI,38	16.76	0.59	I, 50	19.27	0.35
76	13.29	1.18	3	11.01	0.74	20	14.64	0.68	18	**14.41**	0.38	39	15.16	0.68	51	17.47	0.66
77	15.60	0.24	4	16.90	0.72	21	16.80	0.64	20	15.6,	**0.27**	40	15.57	0.30	52	18.48	0.55
78	15.25	0.48	5	16.35	0.66	24	15.78	0.70	23	17.21	**0.67**	41	16.64	0.67	53	19.06	0.36
79	15.66	0.30	6	15.74	-0.13	25	13.62	1.01	24	15.90	0.68	42	15.54	0.72	54	18.58	0.52
I, 80	15.38	0.59	III, 7	16.44	0.63	IV 26	16.32	0.7,	V, 26	15.38	0.41	VI,43	15.53	0.69	I, 55	18.66	0.47
81	13.86	0.96	8	15.43	0.64	27	14.03	0.88	27	17.11	0.58	44	17.07	0.57	57	18.51	0.52
82	16.31	0.59	9	15.63	0.23	28	15.44	0.69	28	17.31	0.58	45	15.66	0.70	58	19.03	0.41
83	15.74	0.63	10	15.99	0.66	29	15.56	0.36	29	**17.32**	0.63	46	17.61	0.53	59	18.94	0.35
84	15.60	0.60	11	17.13	0.65	30	15.02	0.70	30	16.58	0.62	47	16.51	0.65	60	18.07	0.55
I, 85	15.98	0.66	III,12	16.47	-0.18	IV, 31	15.83	0.71	V, 31	16.65	0.61	VI,48	15.90	-0.17	I, 61	17.00	0.63
86	16.16	-0.2,	13	16.57	0.66	32	15.22	0.45	32	15.50	0.96	49	15.78	-0.11	62	18.95	0.40
87	13.54	1.04	14	15.73	-0.12	33	15.68	0.18	33	15.47	0.68	50	15.90	0.66	63	19.06	0.41
88	15.60	-0.09	15	15.19	0.73	34	17.82	0.08	34	16.73	0.59	51	17.08	0.71	64	19.37	0.36
89	16.17	0.64	18	15.37	0.66	35	17.31	0.67	35	16.85	0.57	52	14.85	0.71	65	18.71	0.53
I, 91	12.63	0.00	III,19	15.50	0.19	IV, 36	15.67	0.62	V, 36	17.35	0 56	VI,54	17.28	-0.39	I, 66	19.12	0.47
92	14.69	0.64	20	15.03	0.65	37	15.97	0.66	37	18.11	-0.81	55	15.57	0.31	67	19.29	0.38
93	15.81	0.65	21	16.33	0.63	38	15.42	0.32	38	17.10	0.69	56	16.08	-0.20	68	19.02	0.39
94	15.44	0.68	22	15.75	-0.16	39	16.75	0.66	39	15.99	0.70	57	17.06	0.64	69	19.20	0.44
96	15.86	-0.14	23	16.31	0.65	40	16.07	0.5?	40	15.84	0.66	58	15.59	0.33	70	16.78	0.59
I, 97	15.76	-0.05	III,25	13.87	0.69	IV, 41	17.54	0.79	V, 41	13.84	0.79	VI,59	14.77	0.61	I, 71	18.22	0.65
98	16.17	0.60	26	16.26	0.71	42	14.67	0.75	42	18.11	0.01	60	16.33	0.68	72	18.68	0.56
100	12.66	0.23	28	10.74	1.35	43	16.66	0.68	43	15.81	-0.15	61	17.13	0.77	73	18.36	0.61
102	16.22	0.66	29	16.58	0.56	44	15.30	0.63	44	17.01	0.67	62	17.17	0.75	74	18.34	0.15
103	15.53	-0.03	30	15.58	0.65	45	17.23	0.58	45	15.05	0.76	63	14.83	0.63	75	18.59	0.54
I, 104	15.63	0.35	III,32	15.41	0.47	IV, 46	16.19	0.59	V, 46	16.45	0.64	VI,64	14.78	0.79	I, 76	19.04	0.44
105	15.47	0.66	33	14.42	0.84	47	15.54	0.43	48	15.66	0.58	65	16.94	0.59	77	18.97	0.48
106	14.03	0.97	34	16.98	0.66	48	15.21	0.67	50	16.70	0.61	66	17.11	0.71	78	17.44	0.68
107	14.66	0.80	35	15.87	0.66	49	17.08	0.65	51	15.45	0.70	67	15 39	0.69	79	18.10	0.71
108	13.30	1.20	36	17.58	0.05	50	15.60	0.22	52	17.25	0.62	68	15.31	0.66	80	16.59	0.90
I, 109	12.70	1.35	III,38	16.86	0.74	IV, 51	15.90	0.59	V, 53	16.65	0.66	VI,69	16.28	-0.21	I, 81	17.70	0.66
			39	13.61	0.25	52	15.38	0.61	54	16.77	0.62	70	16.19	0.64	82	19.12	0.42
			41	16.96	0.55	53	13.85	0.63	55	16.92	0.64	71	16.30	0.62	84	16.70	0.61
			42	17.12	0.58	55	16.64	0.59	56	17.15	0.58	72	15.16	0.77	94	17.47	0.73
			43	15.48	0.58	56	15.70	0.11	57	17.02	0.55	73	15.91	0.13	95	19.60	0.48

TABLE 6 (Cont'd)

No.	m_{pv}	CI	No.	m_{pv}	CI	No.	m_{pv}	CI	No.	m_{pv}	CI	No.	m_{pv}	CI	No.	m_{pv}	CI
I, 97	17.72	0.67	III,25	17.05	0.61	V, 30	17.89	0.65	VI, 78	17.04	0.70	1, 228	19.65	0.39	II,188	20.25	0.45
98	17.19	0.67	26	17.50	0.66	31	18.40	0.62	80	17.75	0.72	231	20.94	0.48	189	19.95	0.51
99	17.80	0.61	27	18.60	0.54	32	18.58	0.52	82	17.69	0.71	233	20.73	0.37	190	20.60	0.60
100	18.44	0.54	28	18.84	0.36	33	18.50	0.51	83	18.53	0.51	235	20.64	0.56	191	20.42	0.57
101	17.28	0.70	29	18.06	0.69	36	18.54	0.58	84	18.19	0.64				192	20.90	0.60
I,102	18.53	0.51	III,30	16.81	0.59	V, 37	18.73	0.52	VI, 85	17.44	0.73	II, 4	20.51	0.55	II,194	20.38	0.44
103	17.99	0.67	31	18.65	0.49	38	18.94	0.45				5	19.75	0.41	195	19.06	0.31
104	16.98	0.65	32	18.63	0.37	39	18.59	0.70		Series III		8	20.61	0.47	197	21.16	0.52
			33	17.87	0.58	40	18.76	0.43				10	20.41	0.49	198	19.62	0.33
			34	18.75	0.53	41	17.86	0.71	18.8 < m_{pv} < 21.2			11	19.99	0.45	199	19.18	0.31
II, 3	18.40	0.03	III,35	19.19	0.42	V, 42	17.87	0.69	I, 10	20.64	0.46	II, 15	20.52	0.59	II,200	19.93	0.37
4	18.97	0.44	43	17.68	0.59	44	18.54	0.55	11	20.42	0.59	18	18.52	0.04	202	20.27	0.47
5	18.50	0.62	44	17.08	0.63	45	18.49	0.63	20	19.27	0.36	19	19.68	0.52	206	20.59	0.61
6	18.99	0.43	45	18.09	0.54	46	18.62	0.58	36	18.49	0.25	21	21.05	0.53	207	20.08	0.39
8	18.42	0.57	46	17.83	0.64	47	18.70	0.43	37	19.25	0.34	22	20.95	0.49	209	20.69	0.57
II, 9	17.32	0.62	III,47	17.09	0.68	V, 48	18.52	0.64	I, 38	19.42	0.43	II, 23	21.13	0.53	II,212	18.30	0.37
10	17.97	0.66	48	17.00	0.63	49	18.92	0.45	40	20.28	0.47	24	20.97	0.53	215	20.86	0.57
11	18.85	0.39	49	17.14	0.64	50	18.60	0.59	42	19.29	0.38	25	19.86	0.39	216	19.46	0.40
12	18.70	0.43	50	17.47	0.66	51	19.02	0.47	44	18.90	0.39	30	21.21	0.43	217	18.52	0.72
13	18.50	0.57	51	17.53	0.63	53	18.50	0.74	45	20.09	0.45	31	20.86	0.40	218	20.74	0.58
II,14	18.85	0.35	III,52	16.90	0.62	V, 62	17.48	0.69	I, 46	19.88	0.41	II, 32	19.91	0.31	II,222	20.14	0.45
15	17.21	0.63				63	17.05	0.71	48	19.13	0.34	35	19.60	0.43	223	20.13	0.36
16	18.65	0.46				65	17.83	0.66	49	19.11	0.38	37	20.67	0.57	224	20.76	0.44
17	19.15	0.34				66	18.26	0.66	51	18.92	0.34	40	21.04	0.57	225	20.70	0.48
18	18.64	0.41				68	18.16	0.39	52	20.22	0.56	51	20.12	0.49	227	20.70	0.52
II,19	16.49	0.56	IV, 1	18.26	0.69	V, 69	17.72	0.50	I, 53	20.07	0.44	II, 60	19.72	0.41	II,228	20.46	0.44
20	18.04	0.66	2	18.71	0.46				56	20.47	0.43	61	20.56	0.52	230	18.91	0.37
24	18.79	0.37	3	18.86	0.45				57	19.29	0.30	63	20.93	0.51	231	20.45	0.53
25	18.98	0.35	4	18.68	0.43				66	19.85	0.51	64	19.87	0.38	232	18.97	0.46
26	18.89	0.37	5	18.42	0.52				68	18.87	0.37	65	20.32	0.52	235	20.02	0.35
II,27	17.83	0.63	IV, 7	18.86	0.50	VI, 1	18.27	0.66	I, 69	20.03	0.48	II, 69	20.77	0.52	II,239	19.15	0.31
28	18.94	0.35	9	17.52	0.70	2	18.24	0.25	71	19.17	0.37	79	21.12	0.50	240	20.07	0.38
29	17.89	0.04	12	17.72	0.07	3	17.61	0.63	72	19.78	0.42	80	21.01	0.60	244	20.52	0.66
30	17.13	0.59	13	18.50	0.63	4	17.72	0.63	73	20.70	0.49	81	20.77	0.57	245	20.04	0.45
32	19.13	0.36	14	19.13	0.43	6	18.90	0.46	76	19.54	0.43	82	21.16	0.58	248	19.71	0.54
II,33	17.24	0.73	IV, 16	17.12	0.69	VI, 7	18.84	0.45	I, 78	19.94	0.40	II, 87	19.84	0.40	II,249	21.03	0.57
34	18.05	0.67	18	19.02	0.47	8	18.60	0.52	80	20.27	0.54	90	19.04	0.43	251	19.31	0.39
35	17.41	0.72	20	18.90	0.48	9	16.76	0.59	84	18.62	0.32	92	19.11	0.32	252	18.89	0.41
37	18.16	0.38	21	18.51	0.62	10	18.40	0.65	85	20.17	0.40	93	20.16	0.49	253	20.95	0.53
38	17.53	0.67	22	17.84	0.73	11	18.57	0.50	86	19.44	0.31	94	20.68	0.51	254	19.53	0.39
II,40	18.31	0.81	IV, 23	18.24	0.71	VI, 12	18.78	0.49	I, 87	19.03	0.31	II, 95	20.14	0.46	II,255	19.68	0.59
41	18.00	0.59	24	19.19	0.43	13	18.95	0.38	88	18.78	0.57	96	19.94	0.44	257	20.13	0.49
42	18.95	0.40	25	18.85	0.50	14	18.89	0.45	91	20.51	0.50	97	20.61	0.71	258	18.91	0.38
43	19.00	0.41	26	19.37	0.40	15	18.33	0.64	92	21.02	0.57	98	19.96	0.43	259	19.91	0.45
45	18.88	0.44	27	19.13	0.46	16	18.32	0.65	101	19.37	0.41	99	20.59	0.46	260	19.49	0.41
II,46	18.60	0.52	IV, 28	17.23	0.88	VI, 17	18.55	0.62	I, 102	19.07	0.47	II,100	19.09	0.67	II,264	19.57	0.38
47	19.16	0.41	29	18.16	0.71	18	19.16	0.45	103	19.99	0.41	102	20.69	0.48	265	20.02	0.44
48	18.76	0.49	31	18.18	0.77	19	19.16	0.41	106	20.04	0.36	105	20.85	0.55	266	19.59	0.43
49	18.61	0.57	32	18.59	0.65	20	16.52	0.45	109	18.77	0.35	106	20.39	0.42	267	20.50	0.53
51	18.64	0.24	33	18.86	0.49	21	18.82	0.45	113	20.78	0.51	108	17.50	0.52	268	20.73	0.46
II,53	19.20	0.35	IV, 34	19.18	0.45	VI, 22	18.90	0.45	I, 114	19.56	0.46	II,109	20.70	0.58	II,272	19.41	1.73
54	18.94	0.38	35	18.67	0.69	23	18.56	0.55	115	20.50	0.49	112	20.35	0.45	273	19.39	0.34
55	18.56	0.37	36	18.09	0.50	27	17.76	0.69	117	19.80	0.48	113	19.82	0.43	275	19.08	0.37
56	18.94	0.37	38	18.96	0.44	28	18.64	0.50	118	20.86	0.51	116	20.44	0.52	276	20.82	0.61
57	18.70	0.49	39	18.75	0.57	29	18.82	0.48	127	20.49	0.59	117	21.07	0.58	282	20.75	0.52
II,58	18.04	0.11	IV, 40	17.53	0.72	VI, 30	18.72	0.48	I, 137	18.66	0.49	II,122	20.75	0.50	II,283	18.89	0.38
59	18.44	0.56	41	18.83	0.46	31	18.93	0.46	140	20.57	0.46	124	20.24	0.58	284	20.92	0.54
60	17.25	0.61	43	18.97	0.44	32	17.19	0.71	142	19.05	0.38	126	17.31	0.58	285	20.38	0.51
61	17.24	0.69	44	19.31	0.44	34	17.39	0.69	145	19.45	0.36	127	20.30	0.54	286	20.30	0.37
69	17.48	0.69	46	19.12	0.46	35	19.04	0.48	150	20.57	0.41	128	20.54	0.50	290	19.63	0.50
II,71	17.50	0.74	IV, 47	16.72	0.70	VI, 36	18.72	0.50	I, 151	19.03	0.34	II,129	21.00	0.53	II,291	19.89	0.47
72	17.00	0.58	55	18.00	0.68	37	19.11	0.28	152	19.63	0.43	130	20.92	0.56	292	20.15	0.64
73	18.09	0.59	56	17.83	0.72	38	19.05	0.47	153	20.04	0.45	131	20.25	0.60	294	19.84	0.52
74	18.62	0.45	61	17.63	0.68	39	19.26	0.43	154	20.51	0.47	134	20.76	0.63	295	20.74	0.59
75	18.48	0.36	63	17.04	0.65	40	18.50	0.61	155	20.73	0.48	136	20.10	0.47	296	19.96	0.43
II,77	18.40	0.27	IV, 64	17.86	0.14	VI, 41	17.28	1.81	I, 156	20.29	0.48	II,140	20.75	0.49	II,297	19.79	0.42
78	17.65	0.59	66	17.50	0.74	42	19.02	0.45	161	19.92	0.53	141	20.37	0.44	299	18.25	0.48
80	16.92	0.70	67	17.80	0.73	43	18.83	0.54	162	20.32	0.53	142	21.19	0.56	300	19.94	0.48
			68	18.12	0.71	45	18.92	0.50	171	19.07	0.37	143	21.02	0.49	304	19.21	0.37
			69	18.02	0.69	46	19.36	0.45	172	19.23	0.40	146	20.03	0.47	306	17.44	0.56
III,1	18.01	0.66	V, 1	17.72	0.71	VI, 47	18.62	0.63	I, 175	19.58	0.40	II,150	20.74	0.50	II,308	20.41	0.53
2	18.52	0.52	6	17.61	0.70	48	19.06	0.51	177	20.49	0.50	153	20.74	0.52	309	20.21	0.46
3	16.92	0.63	7	17.76	0.69	49	19.22	0.51	190	20.18	0.49	154	19.56	0.36	314	19.97	0.40
4	16.88	0.61	8	18.56	0.47	50	19.26	0.48	191	19.97	0.51	155	19.15	0.40	315	19.99	0.44
5	18.08	0.63	9	18.89	0.42	52	17.92	0.67	192	20.32	0.42	161	20.83	0.56	316	21.09	0.54
III,6	18.76	0.41	V, 10	17.47	0.94	VI, 53	16.94	0.62	I, 193	19.94	0.47	II,162	20.20	0.41	II,317	19.20	0.47
8	17.89	0.62	11	18.88	0.43	54	17.51	0.60	194	19.68	0.45	164	19.18	0.44	325	18.02	0.54
9	18.48	0.29	13	17.40	0.65	55	18.67	0.53	195	19.04	0.26	167	18.80	0.38	326	21.13	0.65
10	17.20	0.63	16	18.70	0.47	56	18.72	0.49	196	19.97	0.41	168	20.62	0.51	327	20.82	0.65
11	18.58	0.46	17	17.22	0.65	57	19.20	0.47	199	18.65	0.50	169	20.17	0.49	328	20.29	0.59
III,12	17.95	0.62	V, 18	16.58	0.63	VI, 58	17.94	0.67	I, 204	19.56	0.38	II,173	20.90	0.47	II,332	19.41	0.42
14	18.59	0.44	19	17.57	0.65	59	17.98	0.50	205	18.92	0.46	176	19.91	0.37	337	20.08	0.48
16	17.43	0.65	20	16.69	0.53	61	17.50	0.67	206	18.98	0.44	178	21.38	0.43	338	19.68	0.41
17	19.12	0.35	21	18.14	0.62	62	17.90	0.65	208	19.80	0.55	179	19.99	0.49	344	18.97	0.40
18	18.70	0.37	22	17.12	0.55	66	17.66	0.67	210	19.73	0.44	181	18.31	0.46	345	19.40	0.50
III,19	18.98	0.27	V, 23	16.74	0.61	VI, 72	17.50	0.65	I, 223	19.88	0.32	II,182	20.06	0.43			
20	18.92	0.37	25	18.37	0.66	74	17.76	0.58	224	20.51	0.44	183	20.62	0.50			
21	18.83	0.38	26	17.98	0.66	75	17.45	0.70	225	20.03	0.40	184	20.25	0.55			
22	17.92	0.57	27	18.84	0.56	76	17.72	0.69	226	20.33	0.50	186	20.42	0.50			
23	17.83	0.46	28	18.72	0.49	77	17.01	0.66	227	19.02	0.39	187	21.20	0.59			

a homogeneous sample since the areas sampled for the three different magnitude intervals were different. Breaks in the frequency function of the plotted points occur at $m_{pv} = 17.5$ and $m_{pv} = 18.8$. This diagram therefore cannot be used to estimate a relative luminosity function.* The ordinate is apparent photovisual magnitude (m_{pv}). The abscissa is the color index (CI) on the system of the photographic materials. The general features of the diagram are similar to those found for M92[6]. There is a well defined giant sequence, a horizontal sequence situated in the Hertzsprung-Russell gap, transition and subgiant sequences, and finally a heavily populated globular cluster main sequence. Although the main sequence was found in the photometry of M92[6], the length of the segment obtained was uncomfortably short. The M3 data, reaching fainter magnitudes, embrace a longer portion of the main sequence thereby definitely establishing its presence.

As in M92, there exists a well defined gap in the horizontal branch of M3 extending from CI = $0^m.00$ to $0^m.18$ (P-V = $+0^m.05$ to $+0^m.22$) which contains no non-variable stars. Furthermore, M. Schwarzschild's earlier

---

* The total luminosity function is however evaluated in the Chapter 2 of this thesis from star counts on plates of differing exposure times.

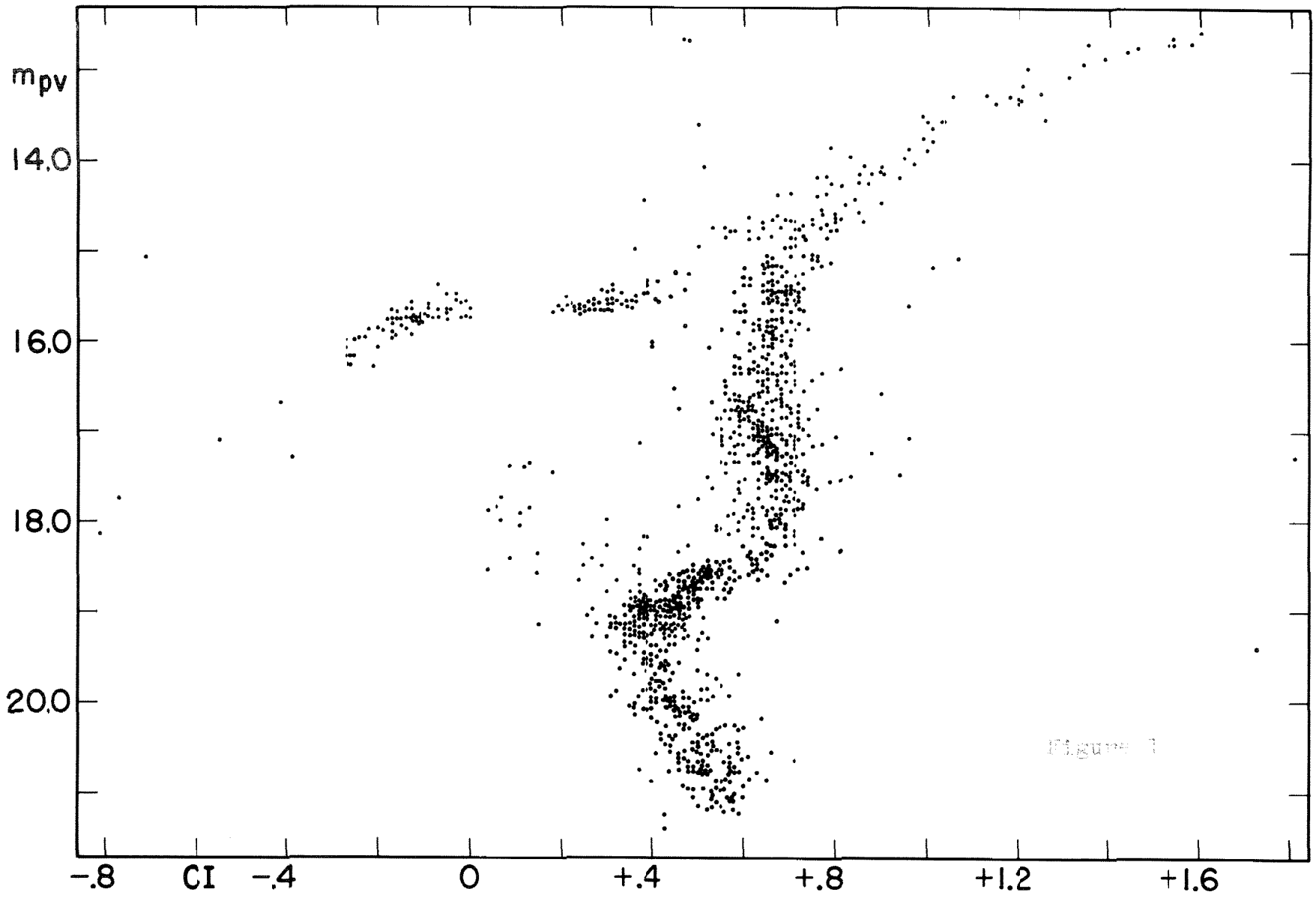
m_{pv}
14.0
16.0
18.0
20.0
−.8
CI
−.4
0
+.4
+.8
+1.2
+1.6

study[16] of M3 shows that probably all the cluster variables are restricted to this distinct region of the H-R plane. This again emphasizes the supposition that a star, to become a cluster type variable, must pass into a well-defined state characterized by definite values of its absolute luminosity and radius.

An additional fact emerges from the present data. It appears that the number of stars per unit color-index interval is continuous along the horizontal branch including the variable star gap. For strict continuity of the density function, the number of variables within the gap should be about 85. (This value was arrived at by considering (1) that the true width of the gap is $0^m.3$ in color index, as indicated by the value of $0^m.2$ shown in Figure 1 and the probable error of $\pm 0^m.02$ in the color index for the non-variable stars at the borders, and (2) that the sixty-five non-variable stars which could not be photometered on series I plates due to excessive crowding would increase the density on both sides of the gap over that shown in Figure 1) The actual number of variables in the cluster area photometered on series 1 plates is 93 which is in good agreement with the 85 required.

Although the diagrams for M3 and M92 are similar in their general features, there are significant differences. A discussion of five of these differences

all shown in Figure 2, follows.

(1) The first difference is the presence in M3 and absence in M92 of the heavily populated region of the horizontal branch immediately to the red of the cluster variable gap. This difference between the two clusters suggests that the presence or absence of the red segment in a given cluster may be correlated with the number of RR Lyrae variables in that cluster. This suggestion follows if the density function along the horizontal branch of all globular clusters is continuous, as the M3 data indicate. The data available for such a correlation of the strength of the red segment with the number of RR Lyrae variables follow: M92 has only 17 variables and the segment is nearly missing, while M3, with 201 variables, has a strong segment. The diagram for M4 by J. L. Greenstein[17] shows a heavily populated red portion of the horizontal branch. M4 has 43 variables. NGC 6397, studied by H. Swope and I. Greenbaum[18], appears to have a very sparse red segment of the horizontal branch and virtually no variables. NGC 6838 (M71), now classified as a globular cluster on the basis of Cuffey's color-magnitude diagram[19], and Mayall's radial velocity measurement[20] apparently has no horizontal branch and no clear case for cluster variables[21]. Unpublished work on the bright stars in M13 by H. C. Arp[22] clearly shows

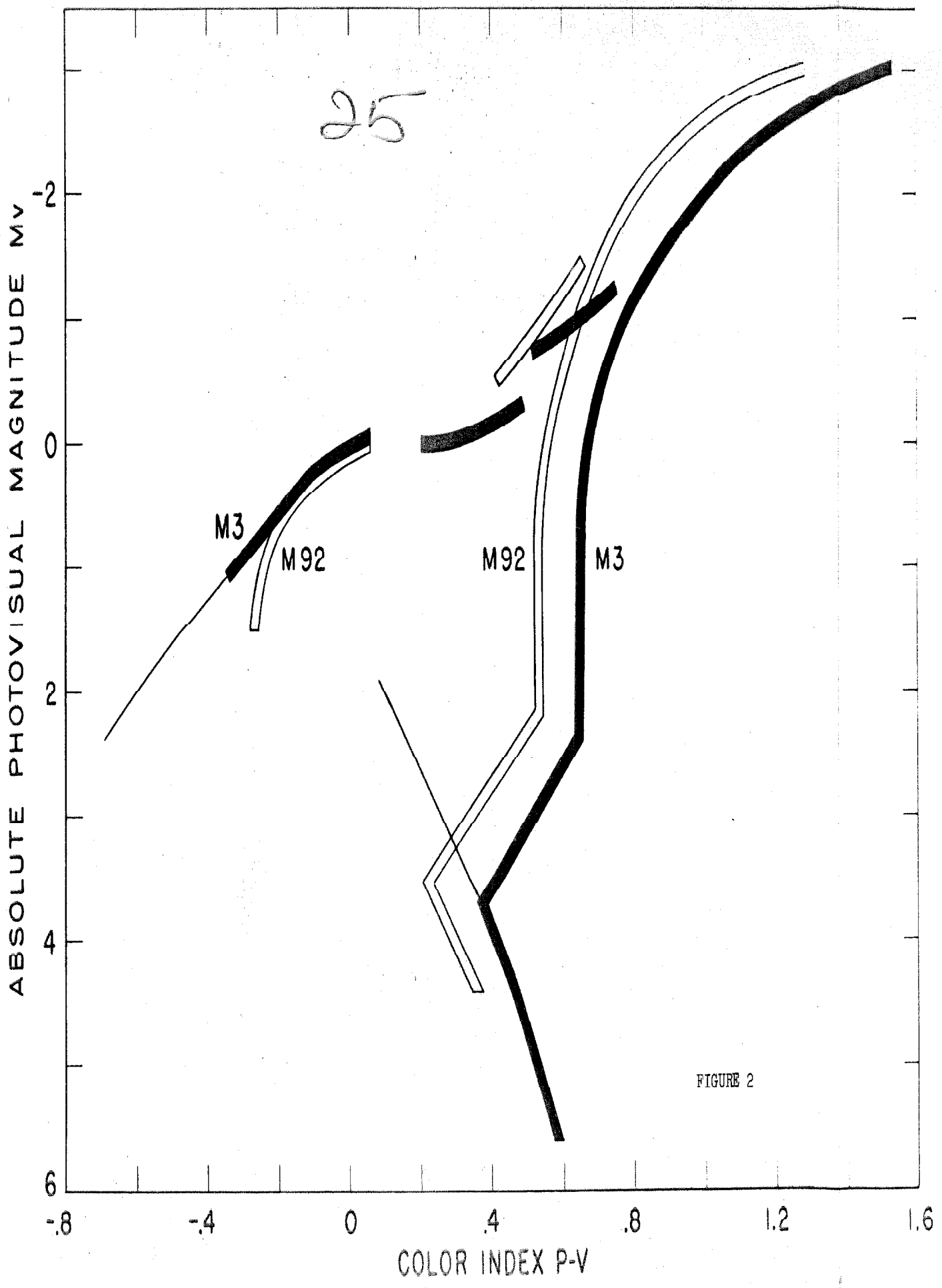
25
ABSOLUTE PHOTOVISUAL MAGNITUDE Mv
-2
0
2
4
6
M3
M92
M92
M3
-.8
-.4
0
.4
.8
1.2
1.6
COLOR INDEX P-V

FIGURE 2

the correlation of few variables and no red segment. M15, studied by Johnson and Schwarzschild[23], is more difficult to judge because of the small number of stars studied. There is, however, an indication of the presence of the red segment. M15 has 74 variables.

(2) The second difference shown in Figure 2 is the extreme blue extension of the horizontal branch in M3 and its absence in M92. Five stars define this extension which reaches $M_V = +2^m.5$ at CI = -0.82. (This absolute magnitude is based on the assumption that the variable star gap is at $M_V = 0^m.0$). Five additional stars which may populate the blue extension were found near the center of M3 with the blink comparator but photometry of these was impossible due to crowding. Stars of this kind seem to be quite rare in the solar neighborhood. One example[24] is undoubtedly BD +28°4211 which has a color index on Harris'[25] system of $-0^m.62$ and, according to Greenstein[26], an absolute visual magnitude based upon interstellar line intensities of from $+3^m$ to $+5^m.5$.

The star in Fig. 1 at $m_{pv} = 15^m.1$, CI = $-0^m.71$ (Series I, II, 57) is identified as a cluster member by its radial velocity which was measured by Popper[27]. Its spectrum is classified by Popper as O8 with no evidence of emission.

Stars in the general field analogous to the blue stars on the horizontal branch of globular clusters are not frequent. However, one group of field stars which seems to be similar are the faint blue stars near the galactic pole whose discovery was announced by Humason and Zwicky in 1946[28]. The identification of these stars with similar stars of known absolute magnitude is of great importance in deciding upon their true space distribution. If they are typical D type main sequence objects, their distances are extremely large. However it is rather certain from unpublished velocity measurements by Humason[29] and from the proper motions by Pels and Perek[30] and Miller and Luyten[31] that the proper identification is with the blue stars of the horizontal branch of globular clusters. This identification gives evidence that the stellar envioronment at large distances above the galactic plane may have population characteristics similar to those of globular clusters.

(3) The third feature which differs in M3 and M92 is the presence in M3 of the globular cluster main sequence brighter than $M_v = +3^m.5$. The stars, shown in Fig. 1, which populate this region cannot be field stars because of their blue color and lack of random distribution. About 34 field stars can be expected[32] in Fig. 1, brighter than $m_{pv} = 17^m.5$. An additional

27 field stars should be found[32] between $m_{pv} = 17^m.5$ to $21^m.0$. These expected numbers are close to the numbers of stars outside the principal sequences in Figure 1, excluding from the count those stars on the main sequence extension.

(4) The fourth and most striking difference between M3 and M92 is the stretching along the CI axis of the M3 diagram as compared with that for M92, resulting in the color differences of the giant, transition, subgiant, and main sequences in the two clusters. This difference in the diagrams was first reported in a preliminary summary concerning part of the present work[33]. Subsequent photoelectric measures[11] have fully confirmed this difference to $M_V = +1$; fainter data rest upon the original calibrations in each cluster. Figure 2 shows that the color difference extends to as faint an absolute magnitude as the diagrams have been carried. Although the giant and dwarf sequences differ in color in the two clusters, the colors of the variable star gaps in each cluster are nearly identical. No intervening interstellar reddening could cause such an effect. The difference must be an intrinsic property of the clusters and very probably results from an internal difference in the stars themselves.

The following suggestion due to M. Schwarzschild[34] offers one explanation for this color shift

in terms of differences in the abundance of the heavy elements between M92 and M3. Consider two stars (one in each cluster) built on the same stellar model and with the same mass but with different internal chemical composition. How will the position of each star differ in a M_{Bol}, log T_e digram? For stars built on the same model

$$\frac{K_0 L R^{0.5}}{M^{5.5} \mu^{7.5}} = \text{const} \qquad (5)$$

where K_0 is the opacity coefficient. If Kramers' opacity law applies, K_0 is directly proportional to the abundance, Z, of the heavy elements which, by hypothesis, differs in the two clusters. The radius, mass and mean molecular weight are the same for both stars. (If Z_{92} and Z_3 are very small, μ essentially does not depend upon Z. The radii of the two stars are the same since their mass and μ are the same and their central temperatures must be identical, otherwise the nuclear energy production would greatly differ between the two stars.) Equation (5) then becomes

$$\frac{L_{92}}{L_3} = \frac{Z_3}{Z_{92}} \qquad (6)$$

Further, since the radii of the two stars are identical,

$$\frac{T_{e,92}}{T_{e,3}} = \left(\frac{L_{92}}{L_3}\right)^{1/4} = \left(\frac{Z_3}{Z_{92}}\right)^{1/4} \qquad (7)$$

Thus both the effective temperature and absolute magnitude will differ for stars of the same mass but of different chemical composition by an amount depending upon $Z_{3/Z92}$. If the systematic difference in the abundance of the metals between the two clusters holds for all their member stars, the entire sequence of stars in one cluster will be displaced relative to the same sequence in the other cluster.

This suggestion, applied to the data of Fig. 4, permits a quantitative evaluation of $Z_{3/92}$. The observations give

$$\log T_{e,92} - \log T_{e,3} = +0.03 \qquad (8)$$

Equation (7) then gives $Z_{3/Z92} = 1.3$ and $\Delta M_{Bol} = +0^m.30$. That is to say, if the metals are 1.3 times more abundant in M3 than in M92, all sequences of stars in M92 built with Kramer's opacity will be shifted toward hotter effective temperatures and higher luminosities. The parallelism of the temperature shift (Fig. 4) in the giant, transition, subgiant, and main sequences supports this explanation. Furthermore there is evidence that the end points of the transition sequence in M92 are about $+0^m.2$ magnitudes brighter than in M3. This is the sense

required by the preceding argument. The above discussion is not valid if electron scattering is the chief source of opacity since κ_o is then independent of Z. In this case the position of sequences in the M_{Bol}, log T_c diagram should be essentially unaltered by a difference of Z. The agreement in position of the horizontal branch in both clusters could therefore be explained if the opacity of stars along this sequence was principally due to electron scattering.

(5) The fifth difference between the two clusters is the disagreement in the slope of the suggested bifurcation in the giant branch at $M_V \simeq -1.0$. Although the evidence for the existence of this feature in both clusters is strong, quantitative agreement of position in the H - R plane does not exist; the M92 segment has the steeper slope.

These five differences between the color-magnitude diagrams of M3 and M92 clearly indicate that all type II systems are not identical.

It is of particular astrophysical interest that the spectra of 14 of the brightest stars in M3 are available from D. M. Popper's work[27]. All of the stars in Popper's list were measured in this investigation and appear with the data in Figure 1. Table 5 gives the results for the photometry of these stars. Although

the stars exhibit no well defined color-spectrum relation, the data do scatter more closely about the luminosity class Ib color-spectrum relation of Eggen[35] (transformed to the P-V system by Johnson and Morgan's transformation[36]) than about any other. Thus it appears that the brightest giants in M3 imitate both the spectrum and color of luminosity class Ib supergiants which are intrinsically 2 magnitudes brighter.

Recent spectral observations with the 200-inch coudé of 11 of the brightest stars in M92 by I. S. Bowen and O. C. Wilson (with classification by Baum[11]), show, however, that the spectral types for these M92 stars are quite different from Popper's spectra for stars of similar color index in M3. The dispersion used by Bowen and Wilson for the M92 observations was 38 A/mm. This is considerably higher than that of 150 A/mm at Hγ used by Popper in his M3 observations. Immediately the question arises whether the differences in the spectra in the two clusters could be an observational effect arising from the difference in dispersion. Bowen, however, obtained a spectrum at 38 A/mm of one of the M3 stars observed by Popper and the spectral classification with the higher dispersion is in good agreement with Popper's result. We must therefore conclude that the observed spectral differences between the clusters are real. At a given color, the M 92 stars are nearly one spectral class earlier than the

Table 5

Photometric Data for Popper's Stars

No. †	Spectral Class Popper †	P	V	Remarks
205	G8 Ib	13.96	12.76	
206	K3 V	10.95	9.86	Not a member
238	K0 Ib	14.15	12.70	
420*	F8 - G0p			
490	G5 Ib	14.10	12.58	
589	G5 Ib	14.19	12.91	
612	Ko Ib	14.15	12.78	
716	G5 Ib	14.53	13.56	
740	G5 IV - V	14.10	13.60	Not a member
752	G8 - K0 Ib	14.08	12.62	
837	G8 Ib	14.12	12.73	
1053	G5 Ib	14.16	12.70	
1127	G8 Ib	14.14	12.97	
1128	O8	14.45	15.04	
1219	G8 Ib	13.99	12.88	
1397	K0 Ib	14.20	12.70	

† Von Zeipel's numbers

* Clearly an optical double on plates taken in fine seeing.

† Ap. J., 105, 204, 1947

M 3 stars.

1.5 Comparison of Population I and II H-R Diagrams

Figure 3 gives the comparison of the M3 diagram with the diagram for type I stars of luminosity class III and V in the solar neighborhood. The zero point for the ordinate scale for M3 was obtained by assuming M_V - 0.0 for the cluster variable gap. The type I sequences were adopted from data kindly furnished by H. Johnson prior to publication. The abscissa values for M3 were obtained from Figure 1 with equation 1 transforming to the P-V system.

Figure 3 shows how the M3 diagram may be used to determine the absolute magnitude of the cluster variable gap. If a positive identification of any portion of the M3 diagram can be made with the similar, trigonometrically calibrated sequence in a diagram containing stars in the solar neighborhood, the two diagrams can be matched and the M_V of the gap determined. There are two sequences in M3 which have their analogue with stars in the solar neighborhood. One is the main sequence and the other is the subgiant sequence. (The subgiant sequence in M3 is that which joins the main sequence at M_V = +3.5.) A straight matching procedure of the M3 main sequence with the luminosity class V main sequence of Figure 3 is uncertain at present for the following four reasons. (1) There is evidence that the type I

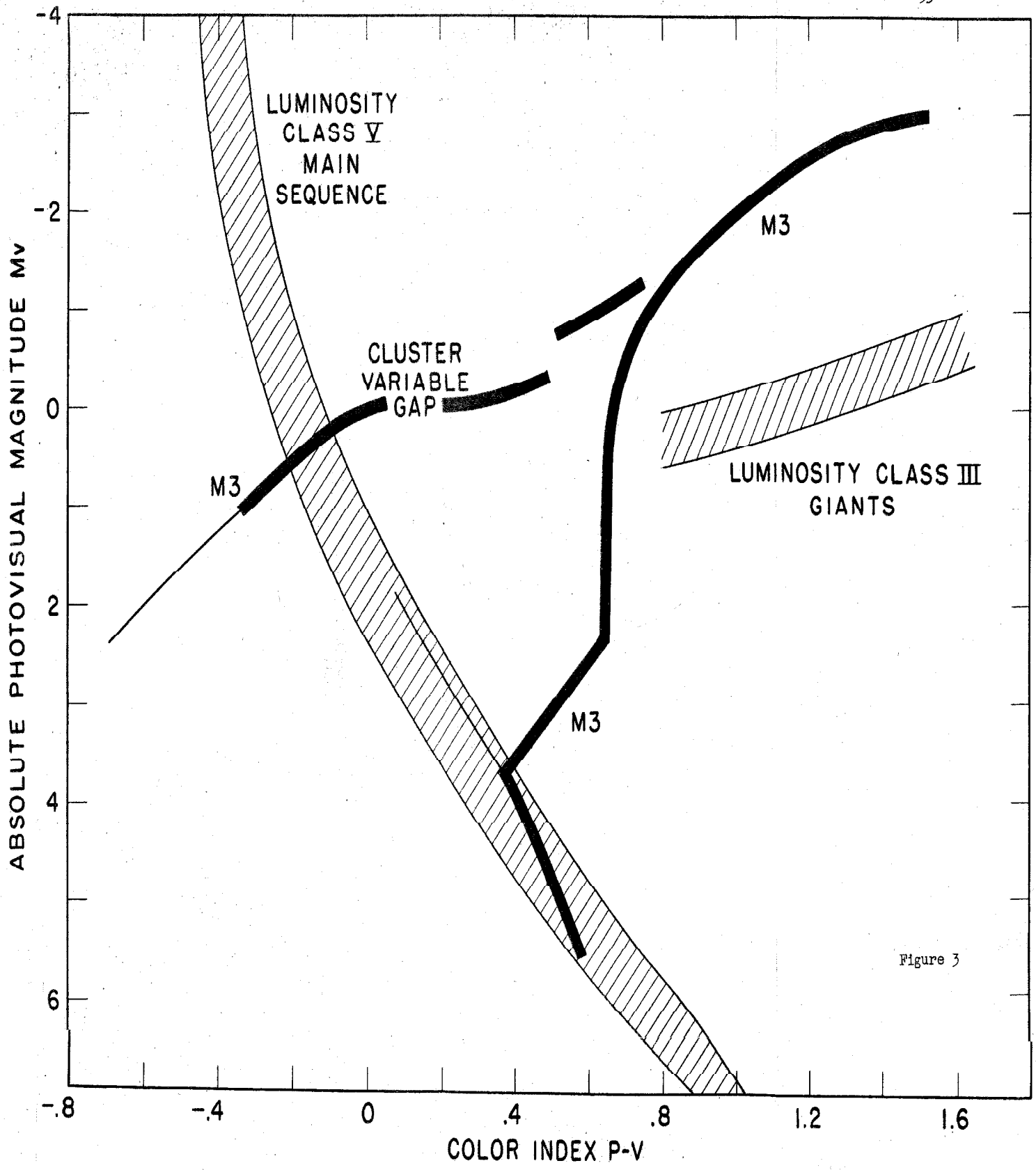
LUMINOSITY
CLASS V
MAIN
SEQUENCE
M3
CLUSTER
VARIABLE
GAP
M3
LUMINOSITY CLASS III
GIANTS
M3
ABSOLUTE PHOTOVISUAL MAGNITUDE Mv
-4
-2
0
2
4
6
-.8
-.4
0
.4
.8
1.2
1.6
COLOR INDEX P-V

Figure 3

and type II main sequences may not be strictly identical in the H-R plane because of possible chemical composition differences in the population species. (2) The globular cluster main sequence may indeed consist of the sub-dwarfs which are suspected to be numerous in the halo region of the galaxy. If this is so, identification of the globular-cluster main sequence with the normal dwarfs will give an incorrect result for M_V. (3) Such a matching procedure is inherently inaccurate because of the extreme accuracy of the color-index required. Along this region of the main sequence $M_V = 6.2\ (P - V) + \text{const.}$ Hence $\delta M_V = 6.2\ \delta\ (P - V)$. A systematic error of only $0^m.03$ in the color index produces an error of $0^m.2$ in the absolute magnitude determination. Interstellar reddening would have the identical effect of an error in CI and the precise evaluation of a color excess to within $\pm 0^m.03$ is quite difficult. (4) Final magnitude calibrations in M3 below $m_{pg} = 19^m.1$ are not yet completed. If the matching were to be done by superposing the main sequence of the two diagrams, little confidence could be placed in the resulting M_V for the cluster cepheids for the above four reasons. However the additional subgiant sequence provides the necessary information to meet all four objects raised above. Olin J. Eggen's diagram[7] for nearby stars contains eight subgiants with trigonometric

parallaxes. When Eggen's material is reduced to the P, V photometric system by the color transformation[36]

$$P-V = 1.205\ C_p^E - 0.065 \qquad (9)$$

the resulting diagram provides an excellent means of superposing the M3 diagram to obtain M_V for all the cluster stars. Objection 1 is overcome since the subgiants are believed to be population II stars and should therefore be of the same species as the subgiant sequence in M3. Objection 2 no longer applies since we are not now dealing with the main sequence. Objection 3 does not enter the argument since we now can fit to the junction of the subgiant and main sequence and therefore shift, if necessary, the diagram along the color axis until the junction points match. Even if the globular cluster main sequence is actually composed of subdwarfs rather than dwarfs, the fit applies since, according to published and unpublished data of Eggen[7], the dwarf and subdwarf sequences cross at $M_V \approx +4.5$ which is the point of interest for this argument. Therefore exact identification of the M3 main sequence is unnecessary for the calibration. Objection 4 does not apply since the magnitudes in M3 are calibrated along the entire subgiant sequence. A fit to Eggen's data gives $M_V = +0.09$ for the cluster variable gap. The uncertainty of this fit is about $\pm 0^m.15$ depending upon personal

judgement of the scatter in both diagrams. This fit to the subgiants is not shown in Figure 3. The figure shows only the fit of the main sequences which gives $M_V = 0.0$. It is therefore evident from these two independent calibrations that the value of $M_V = 0.0$ for the absolute magnitude of the cluster variablesis essentially correct. This new calibration is of importance in a decision on the adoption of a new distance scale to extra-galactic nebulae discussed by W. Baade[37]. The value of $M_V = 0.0$ for the cluster cepheids make it evident that the discrepancy of -1.5 magnitudeswhich appeared when the globular clusters in M 31 were compared by Hubble with those in our own system[38] must be due to an error in the classical cepheid period-luminosity relation zero point from which the distance to M31 is determined. Baade's recent work on M31, together with the re-evaluation of the absolute magnitude of the cluster variable from the M3 color-magnitude diagram rather strongly shows that the distance modulus of M31 and presumably to all extra-galactic nebulae must be increased by about 1.5 magnitudes or a factor of two in distance.

The modulus of $m - M = 15.63$ for M3 together with Figure 1 gives the absolute photovisual magnitude of the brightest stars of the population II as $M_V = -3^m.0$ at $P - V = +1^m.60$. These values are important instudies of the nearest extra-galactic systems

in which the population II can just be resolved.

The color-magnitude diagram of Figure 1 provides the data which eventually must be explained by detailed stellar models. It will therefore be convenient to represent the results of this chapter in the M_{Bol}, log T_e plane since these variables are the ones usually obtained from computations of theoretical models. The M3 color-magnitude diagram is converted to these variables in Figure 4.

The effective temperature scale is that tabulated by Keenan and Morgan[39]. The bolometric corrections are those of Kuiper[40]. Lines of constant radii are also shown in Figure 4. One missing datum of interest in this figure is the lines of constant mass. Nothing yet is known about the mass-luminosity law for type II stars - an obviously important datum from the standpoint of stellar evolution. There is, unfortunately, little hope of obtaining this datum by the ordinary binary methods, since multiple stars seem to be quite rare in type II systems.

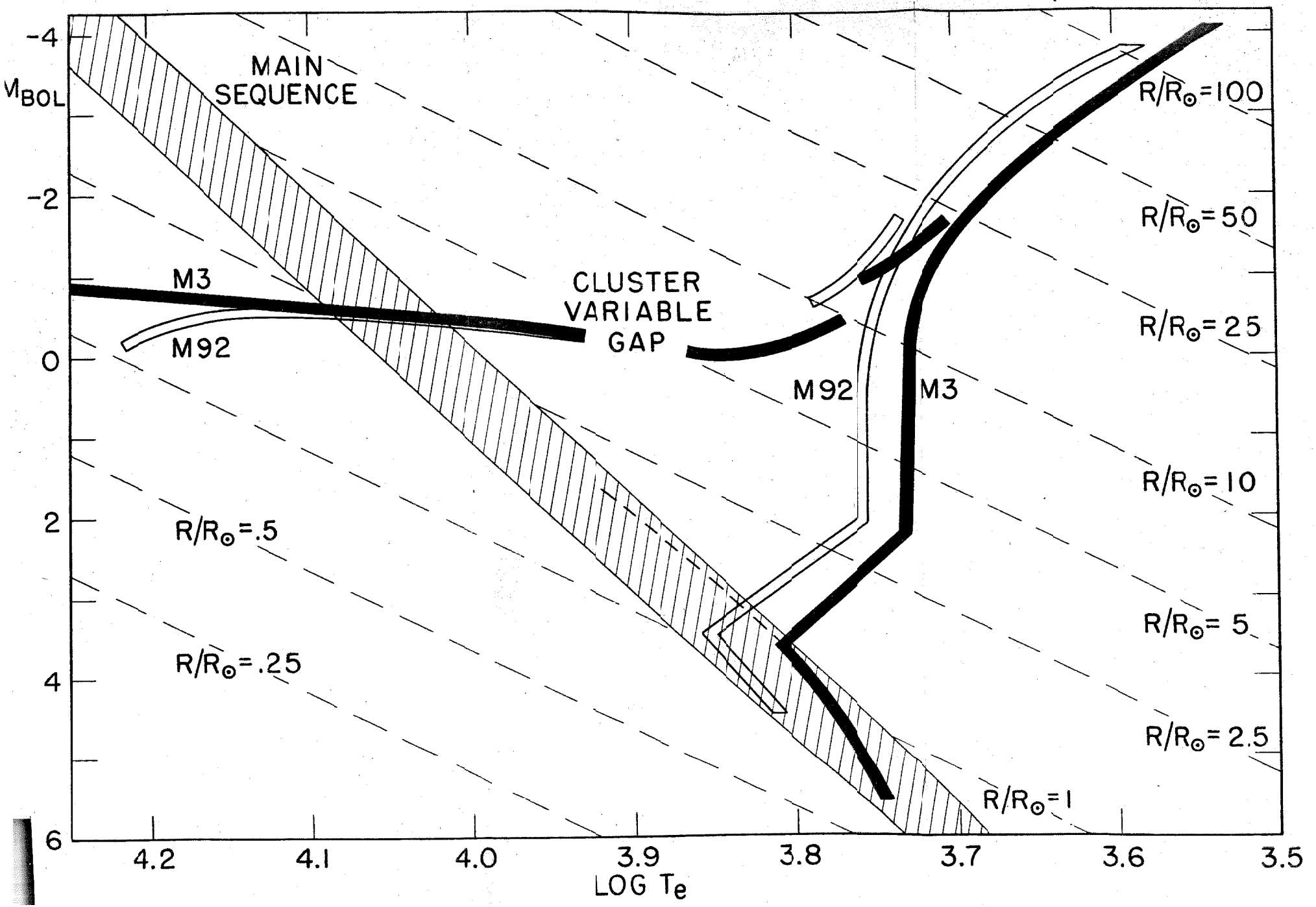
MAIN SEQUENCE
M3
M92
CLUSTER VARIABLE GAP
M92
M3
R/R⊙=100
R/R⊙=50
R/R⊙=25
R/R⊙=10
R/R⊙=5
R/R⊙=2.5
R/R⊙=1
R/R⊙=.5
R/R⊙=.25
M_BOL
-4
-2
0
2
4
6
4.2
4.1
4.0
3.9
3.8
3.7
3.6
3.5
LOG Te

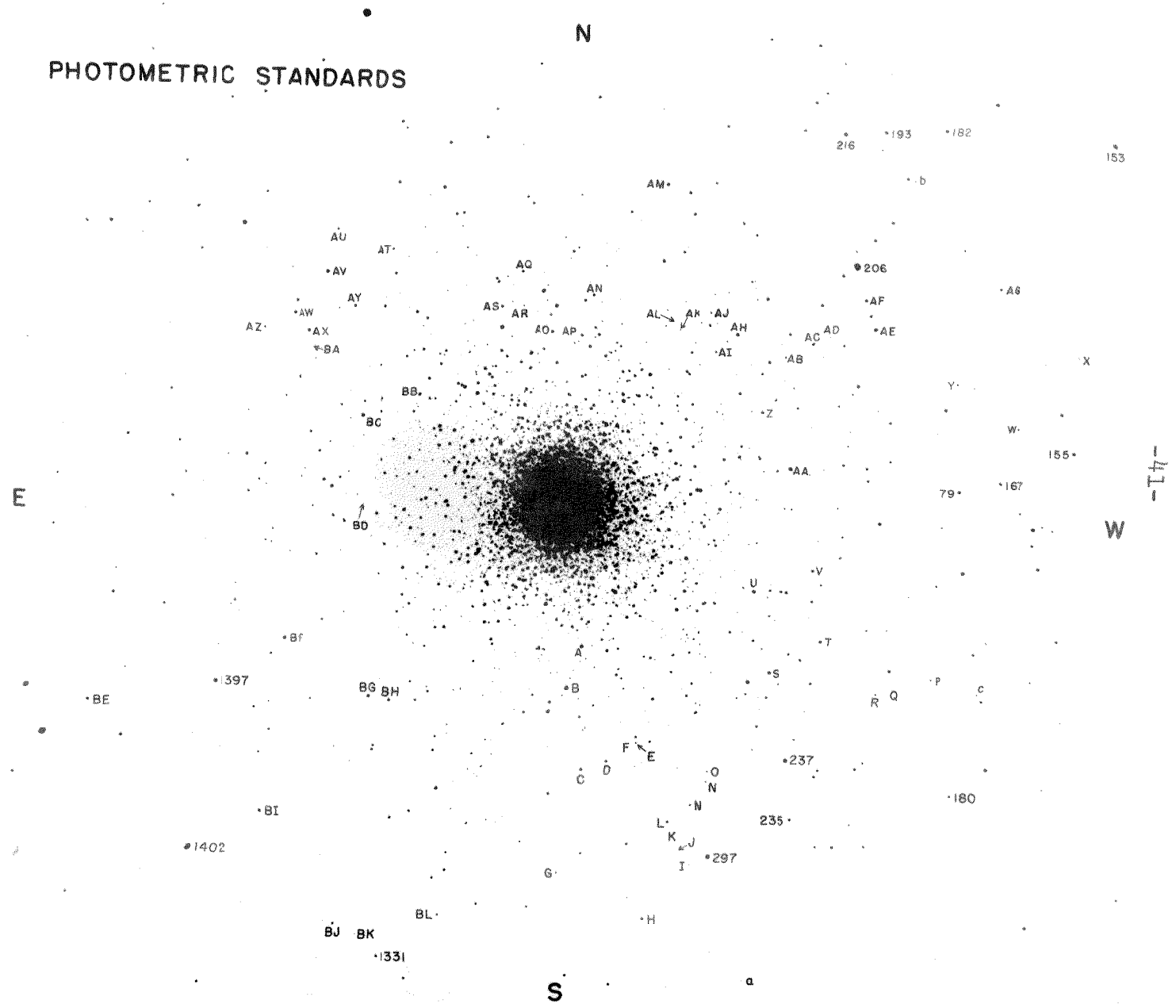
PHOTOMETRIC STANDARDS
N
E
W
S
AM
AU
AT
AV
AQ
AN
AY
AW
AZ
AX
BA
AS
AR
AO
AP
AL
AK
AJ
AH
AI
AF
AE
AD
AC
AB
BB
BC
BD
Z
AA
BE
BF
BG
BH
A
B
C
D
E
F
G
H
I
J
K
L
M
N
O
P
Q
R
S
T
U
V
X
Y
W
a
b
c
216
193
182
153
206
155
167
79
397
237
180
235
297
1402
BI
BL
BJ
BK
1331

Figure 5

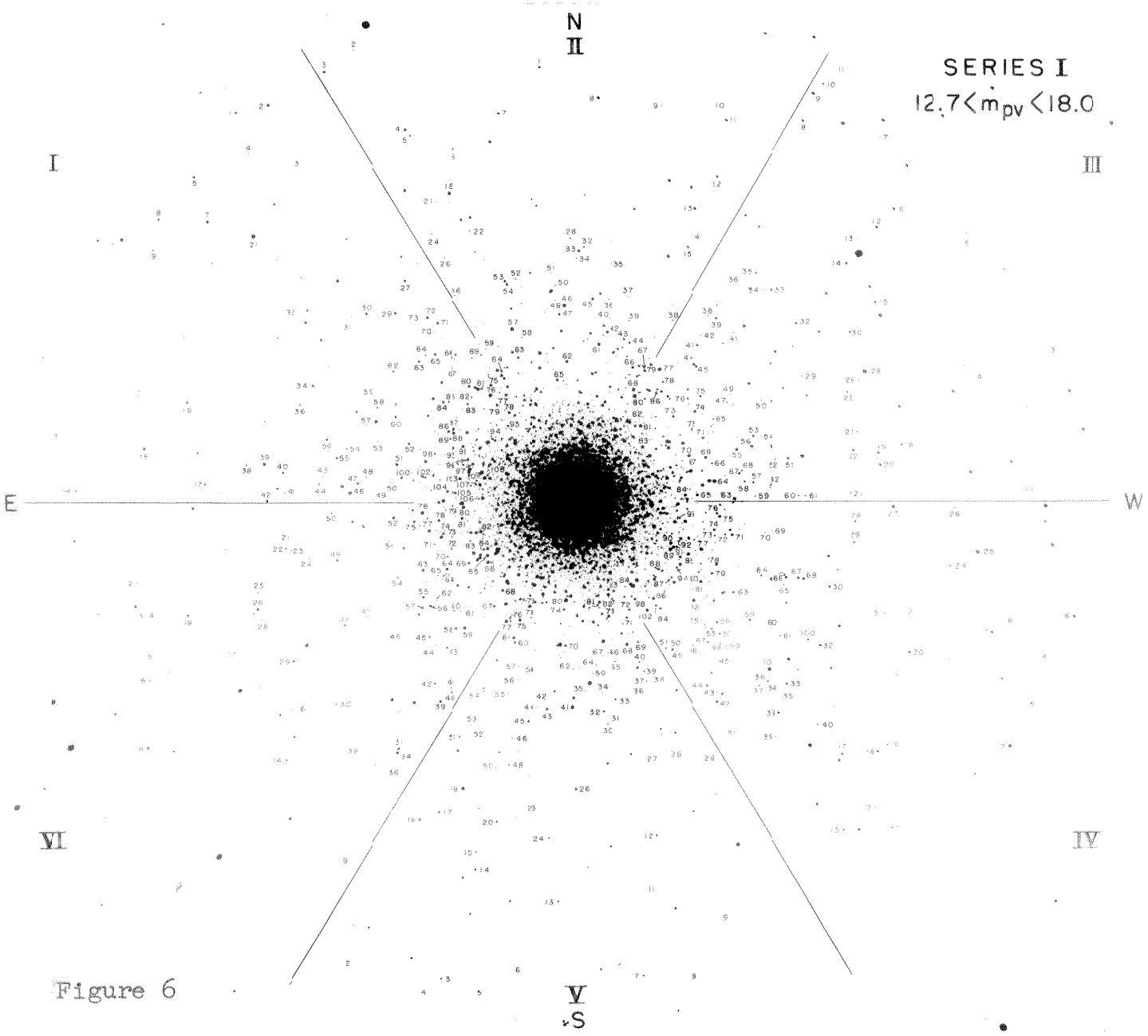

Figure 6

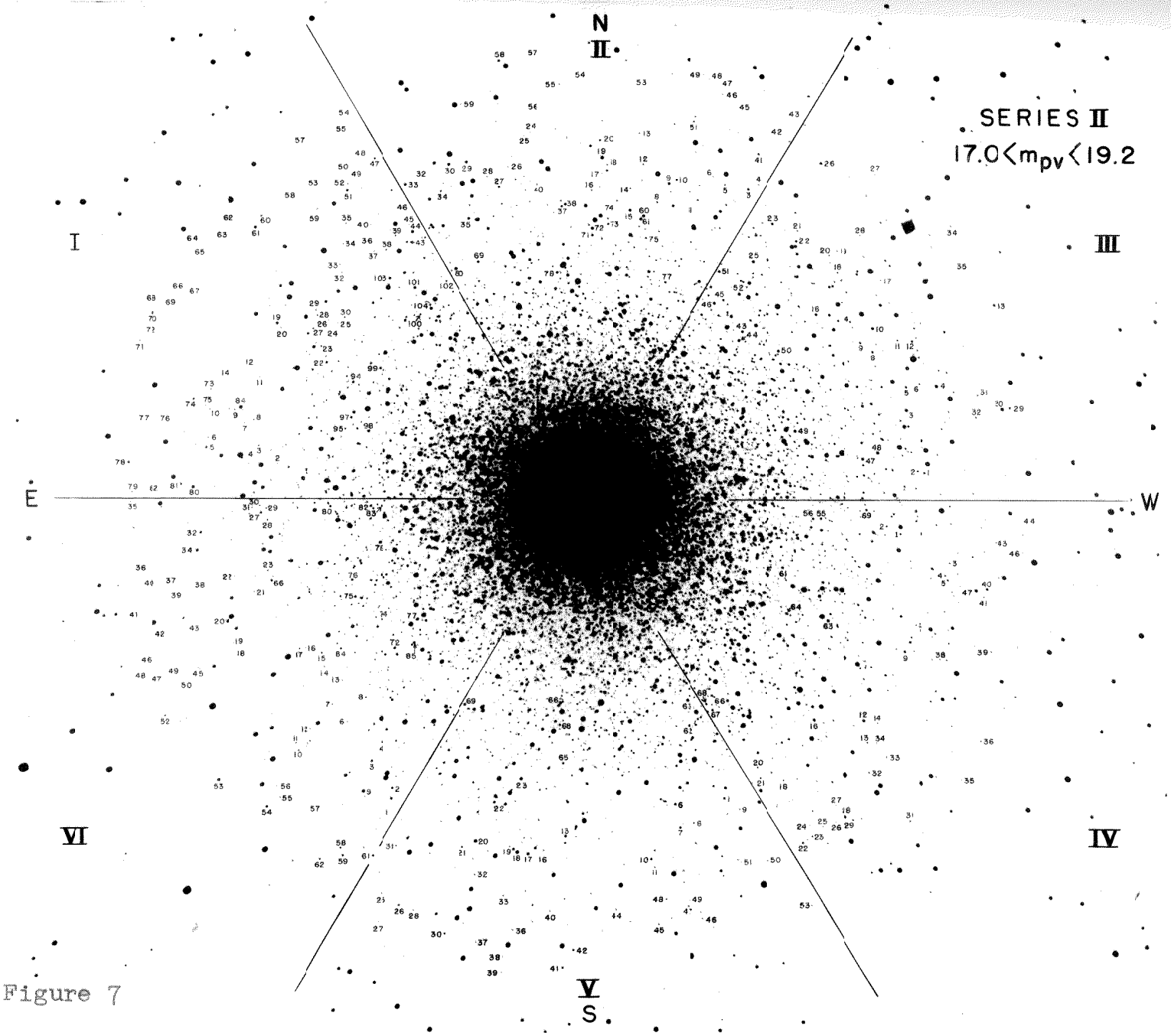

Figure 7

Figure 8

SERIES III

$18.8 < m_{pv} < 21.2$

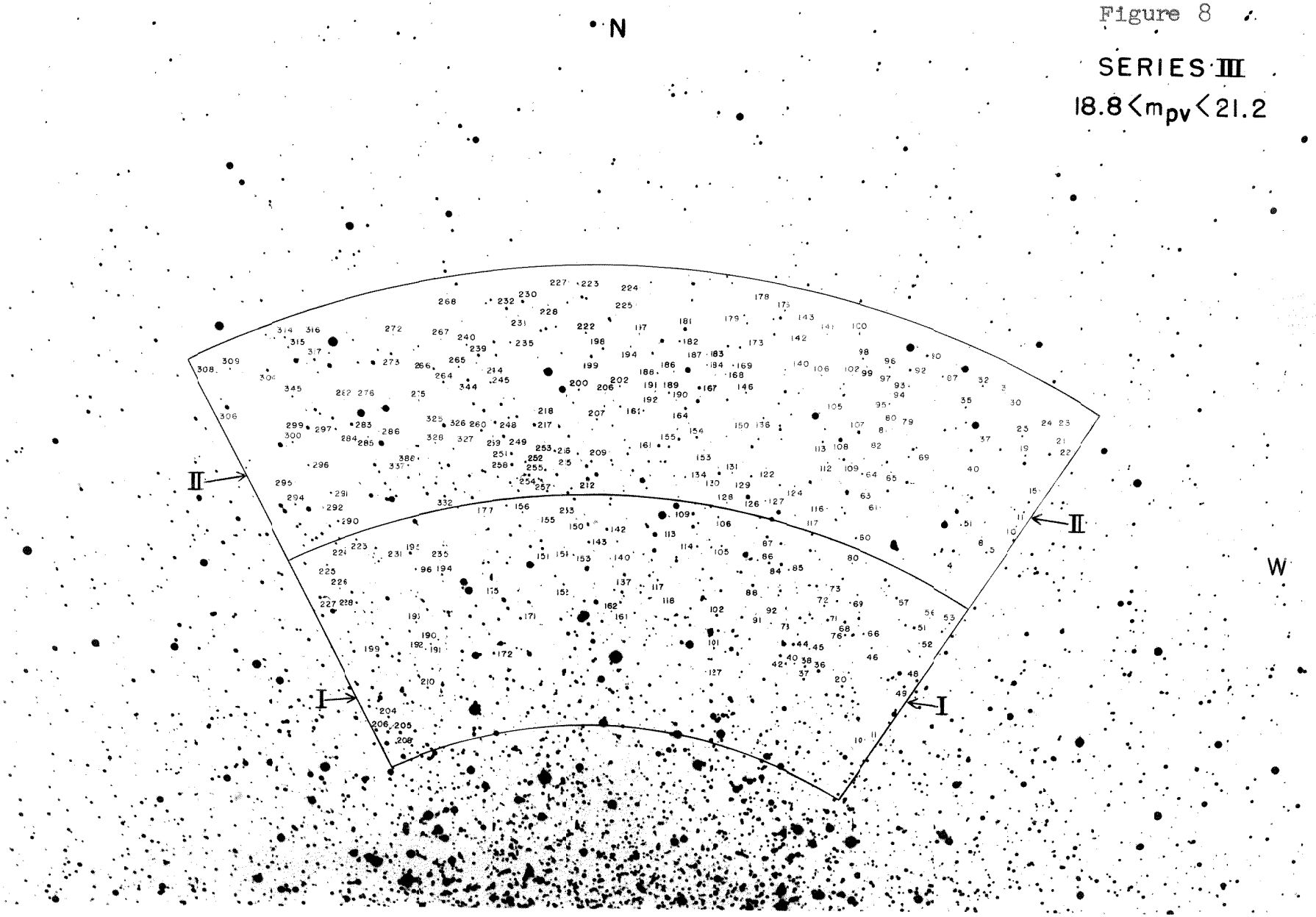

Figure Captions for Chapter 1.

Figure 1. The color-magnitude diagram for M3. All known variable stars were excluded from the photometry. The ordinate and abscissa are on the magnitude and color system of the photographic materials. The transformation to the P and V system of Stebbins, Whitford and Johnson may be made by use of the color equations 1, 2 and 3 given in the text. The diagram does not represent a homogeneous sample. The density of points does not, therefore, give a relative luminosity function.

Figure 2. Comparison of the schematic M3 and M92 color-magnitude diagrams. The black line is the diagram for M3 while the open line is that for M92. No shift in the abscissa values was made for either cluster. Normalization of the ordinate was made by assuming M_v = $0^m.0$ for the cluster variable gap.

Figure 3. Comparison of the M3 diagram with the type I sequences in the solar neighborhood. The population type I data were adopted from unpublished work by H. Johnson which he very kindly made available. No shift in the

abscissa of M3 was made. The zero point for the ordinate scale was found by assuming $M_v = 0^m.0$ for the cluster variable gap.

Figure 4. Comparison of the M3 and M92 diagram with the type I main sequence in the M_{Bol}, log T_e plane. The effective temperature scale is that quoted by Keenan and Morgan. The bolometric corrections are those of Kuiper. Lines of constant radii are shown.

Figure 5. Identification chart for the photometric standards. The stars which are numbered are the photoelectric standards of Table 1. The numbers are Von Zeipel's. Lettered stars are from the secondary standard sequence of Table 2. The faint extrapolated standards are now shown.

Figure 6. Identification chart for the stars of series I $12.7 < m_{pv} < 18.0$. Identifying numbers correspond to those of Table 6, series I.

Figure 7. Identification chart for stars of series II ($17.0 < m_{pv} < 19.2$). Identifying numbers correspond to those of Table 6, series II.

Figure 8. Identification chart for stars of series III ($18.8 < m_{pv} < 21.2$). Identifying numbers correspond to those of Table 6, series III.

References. Introduction and Summary, and Chapter 1.

1. S. I. Bailey, Am.A.S.Pub., 1, 49, 1898
2. W. Baade, Ap.J., 100, 137, 1944
3. W. Baade, P.A.S.P., 60, 230, 1948
4. E. P. Hubble, Proc.Am.Phil.Soc., 95, 461, 1951
5. Annual Report of the Director, Carnegie Instit. of Wash. Yearbook 1950-51
6. Arp, Baum, and Sandage, A.J., 58, 4, 1953
7. O. J. Eggen, Ap.J., 112, 141, 1950
8. Van Rhijn, Groningen Pub. No. 47, 1936
9. W. H. Christie, Ap.J., 91, 8, 1940
10. Stebbins, Whitford, and Johnson, Ap.J., 112, 469, 1950
11. W. A. Baum, A.J., 57, 222, 1952
12. H. von Zeipel, Ann Obs. Paris, Mem 25, 1908
13. L. C. Eichner et al., A.J., 53, 25, 1947
14. Shapley and Davis, Ap.J., 51, 140, 1920
15. Helen Sawyer, Pub David Dunlap Obs., 1, No. 4, 1939
16. M. Schwarzschild, Harv.Circ.,No. 437, 1940
17. J. L. Greenstein, Ap.J., 90, 387, 1939
18. H. Swope and I. Greenbaum, A.J., 57, 83, 1952
19. J. Cuffey, Ap.J., 98, 49, 1943
20. N. U. Mayall, Ap.J., 104, 290, 1946
21. H. B. Sawyer, A.J., 57, 26, 1952

22. H. C. Arp, Private conversation

23. H. Johnson and M. Schwarzschild, Ap.J., 113, 630, 1951.

24. MacRae, Fleischer, and Weston, Ap.J., 113, 432, 1952

25. D. L. Harris, III, Ap.J., 113, 435, 1952

26. J. L. Greenstein, P.A.S.P., 64, 256, 1952

27. D. M. Popper, Ap.J., 105, 204, 1947

28. M. Humason and F. Zwicky, Ap.J., 105, 85, 1947

29. M. L. Humason, Private conversation

30. Pels and Perek, B.A.N. 11, 422, 1951

31. Luyten and Miller, Ap.J., 114, 488, 1951

32. Seares et al., Ap.J., 62, 320, 1925

33. Arp, Baum, and Sandage, A.J., 57, 4, 1952

34. M. Schwarzschild, Private conversation

35. O. J. Eggen, Ap.J., 113, 663, 1951

37. W. Baade, Minutes of Meeting of Commission 28. I.A.U., Rome, September 4-13, 1952

38. E. P. Hubble, Ap.J., 76, 44, 1932

39. Astrophysics, ed by Hynek, McGraw-Hill, 1951 Chapter 1.

40. J. P. Kuiper, Ap.J., 88, 446, 1938

Chapter 2. The Luminosity Function and Radial Density Distribution in M3

2.1 Summary and Conclusions

The luminosity function $\varphi(M)$ to $M_{pg} = +7$ is obtained for M3 from star counts from plates exposed to different limiting magnitudes. Table 8 and Figures 9 and 10 give the data. The characteristic peak at $M = 0.0$ due to the horizontal sequence is conspicuous. The function rises to a maximum at $M_v = +5.5$ and then decreases to as far as the data can be carried. The existence of this maximum is beyond doubt but the exact form of the decrease beyond $M_{pv} = +5.5$ is uncertain for observational reasons. The function must however rise again for magnitudes fainter than $M_{pv} = +7$ to explain the mass of 5.6×10^5 M ⊙ obtained by O. C. Wilson from internal velocity measurements. Arguing from the failure of the Van Rhijn function to provide enough dwarf stars in M3 for a mass of 5.6×10^5 M ⊙, the $\varphi(M)$ is inferred to be larger by a factor of 10 than the $\varphi(M)$ in the solar neighborhood for stars fainter than $M_{pv} = +7$.

Two integral properties-(1) the mass to light ratio and (2) the composite energy distribution curve - are discussed in a comparison between globular clusters and elliptical nebulae. The mass to light ratio of M3 is 2.7 while that of E nebulae about 70-a significantly

different value. Furthermore, Figure 12 shows the great difference in the composite energy distribution curves for the two classes of objects. These facts, together with the large observed differences in the integrated spectra of M3 and M32 show that we are dealing with two basically different classes of objects and suggest a dichotomy in the type II classification. The suggestion is advanced that a separation into disc and halo population II be made. A prediction concerning the integrated spectrum of the globular cluster NGC 6522 follows from this hypothesis.

The projected density distribution is found and given in Table 9 and Figure 13. Inspection of this data shows the presence of segregation of the bright from the faint stars starting at about $M_V = +4$. Stars brighter than this show the same form of $\rho(m, r)$ indicating no systematic trend for segregation of stars from $M_V = -3$ to $+4$. This is significant from an evolutionary standpoint since the absence of a normal mass-luminosity law in M3 for stars brighter than $M = +4$ may possibly be inferred.

2.2 The Determination of $\varphi(m)$

The luminosity function, $\varphi(m)$, defined as the number of stars per unit volume between magnitude $m - 0.1$ and $m + 0.1$ was determined for M3 by two different

methods. (1) For stars brighter than $m_{pv} = 17.0$, the form of $\varphi(m)$ was found from counts in magnitude intervals in Table 6. This is a valid procedure since the catalogue is complete to this magnitude, in a relative sense, because no selective criteria were used in the choice of stars to be measured. However, this relative $\varphi_R(m)$ differs from the total function since not all stars in the cluster could be photometered thus causing Table 6 to be incomplete. (2) For stars fainter than $m_{pv} = 17.0$, not even the form of $\varphi(m)$ could be obtained from Table 6 due to the selectivity involved in the choice of stars below this limit. It is evident, therefore, that fainter than $m_{pv} = 17.0$ data other than that of Table 6 must be used to obtain $\varphi(m)$. These additional data consist of star counts on a series of plates of the cluster exposed to different limiting magnitudes. These counts not only gave $\varphi(m)$ fainter than $m_{pv} = 17.0$ but also the multiplicative factor by which to multiply $\varphi_R(m)$ for the bright stars from Table 6 to obtain the total $\varphi(m)$.

Ten plates were counted, all taken on Eastman 103aD plates behind a Schott GG11 filter with the 200-inch Hale telescope. The limiting magnitudes to which the counts refer were determined for each plate by comparisons

with stars of Table 6. The final N (m) adopted from the counts is given in Table 7. N (m) is defined as the total number of stars in M3 within a radius of 8 minutes of arc from the cluster center brighter than apparent magnitude m.

The difficulty in determining the total N (m) for the cluster arises from the necessity of extrapolating the star counts into the densely packed nuclear region where counts of individual objects are impossible. This difficulty may be appreciated by inspection of Figure 8, Chapter 1. The problem is not, however, as serious as might be imagined since

$$N(m) = 2\pi \int_0^{8'} \rho(m,r)\, r\, dr \qquad (10)$$

The function $\rho(m,r)$ is the number of stars per square minute of arc brighter than magnitude m at a distance r from the center. A rather bad extrapolation of $\rho(m,r)$ as $r \to 0$ has small effect on N (m) since the weighting factor, $\pi \overline{r^2}$, (which is the cluster area over which the extrapolation is necessary) is quite small. For this reason the N (m) obtained from the counts is not subject to large error from the crowding effect. The N (m) values in Table 7 were determined from equation

Table 7

Star Count Data for M3

Plate	Exp. Time	Limit m_{pv}	M_{pv} †	N (m)
PH-350-S	5s	14.1	-1.53	169
PH-351-S	15s	15.0	-0.63	396
PH-353-S	30s	16.1	+0.47	1,318
PH-354-S	1m	16.9	1.27	1,949
PH-352-S	3m	17.7	2.07	2,648
PH-355-S	6m	19.5	3.87	9,812
PH-486-S	5m	20.1	4.47	15,939
PH-613-B*	10m	20.7	5.07	22,175
PH-487-S	15m	21.6	5.97	34,875
PH-385-B*	50m	(22.5)	6.87	44,542

*Plate taken by Baade

† Corresponds with a modulus $m - M = 15.63$ given in Chapter 1.

10 by the extrapolation of $r\rho(m, r)$ as $r \rightarrow 0$.*

The function $\varphi(m)$ is defined as the number of stars in M3 within 8 minutes of the cluster center between apparent magnitude m - 0.1 and m + 0.1. It follows that

$$N(m + 0.1) = \sum_{m_i = -\infty}^{m} \varphi(m_i) \qquad (11)$$

where $m_{i+1} = m_i + 0.2$

Values of $\varphi(m_i)$ may in principle be obtained by differencing the function N (m + 0.1) at the appropriate arguments. However, since N (m + 0.1) is small for the first four magnitude intervals, it is unwise to obtain

---

* The limiting magnitude for the last plate in Table 7 was below the limit of Table 6 and therefore the value of m_{pv} is uncertain. This value was obtained by the experimental rule used at Mount Wilson for many years[1], that for a factor 3 in exposure time, the gain in limiting magnitude is 1.0. A 15 minute exposure with the particular emulsion of the last plate of Table 7 could reach m_{pv} = 21.5. The exposure time of PH-385-B was 50 minutes. Its limiting magnitude would be m_{pv} = 22.5 by the above experimental rule. However the seeing on the particular night that PH-385-B was taken was superb. The exquisite images suggest that the limiting magnitude of this plate is below 22.6. However, because of the uncertainty and in view of the danger of over-discussion of the data, the round figure of m_{pv} = 22.5 will be adopted for this plate.

the bright part of $\varphi(m)$ in this way so the first procedure given on page 51 was used. The form of luminosity function for the bright stars, $\varphi_R(m)$, was obtained from Table 6. This form differs from $\varphi(m)$ only by a multiplicative constant, i.e.

$$\varphi(m) = a \quad \varphi_R(m) \tag{12}$$

where a measures the incompleteness of Table 6. Its value was determined from

$$N(m) = a \; N_R(m) \tag{13}$$

where $N_R(m)$ is known from counts in Table 6 and $N(m)$ from the data of Table 7. The value which best fits the data is $a = 3.5$. This means that Table 6 is incomplete to $m_{pv} = 17.0$ by this factor from containing all the stars in the cluster.

Figure 9 gives the total luminosity function for the brightest stars in M3 determined in this way. The histogram represents counts in Table 6 multiplied by 3.5. The 200 variable stars not included in this table have been added. The characteristic hump at $m_{pv} = 15.6$ ($Mv = 0.0$) is quite conspicuous. When all stars bluer than CI = 0.50 were excluded from the count, the dotted histogram resulted. This shows that

the hump in φ (M) at M_{pv} = 0.0 is caused entirely by the stars on the horizontal branch. The extreme narrowness of this characteristic peak further illustrates the small dispersion in the photovisual magnitudes of most stars on the blue branch. Finally, Figure 9 shows the relative incompleteness of Table 6 fainter than m_{pv} = 17.0.

Fainter than m_{pv} = 17.0, φ(m) was found by differencing equation (11) by taking the values of N (m) from a smoothed curve passing through the data of Table 7. The resulting $\varphi(M_{pv})$ is shown in Figure 10 and given numerically in Table 8 at intervals of 0.2 magnitudes. Also tabulated in the third column of Table 8 are the corresponding values of N (M + 0.1). These values give the total number of stars in M3 brighter than M + 0.1 within 8 minutes from the nucleus.

The luminosity functions in photographic light (M_{pg}) and bolometric light (M_{Bol}) were obtained from the $\varphi(M_{pv})$ values by a suitable application of the color indices and bolometric corrections[2]. These values are also given in Table 8.

It is quite remarkable that a linear relation between log φ (M) and M_{Bol} exists from M_{Bol} = + 1.0 to +4.0. This is of significance since precisely such a relation is required for an evolutionary explanation of

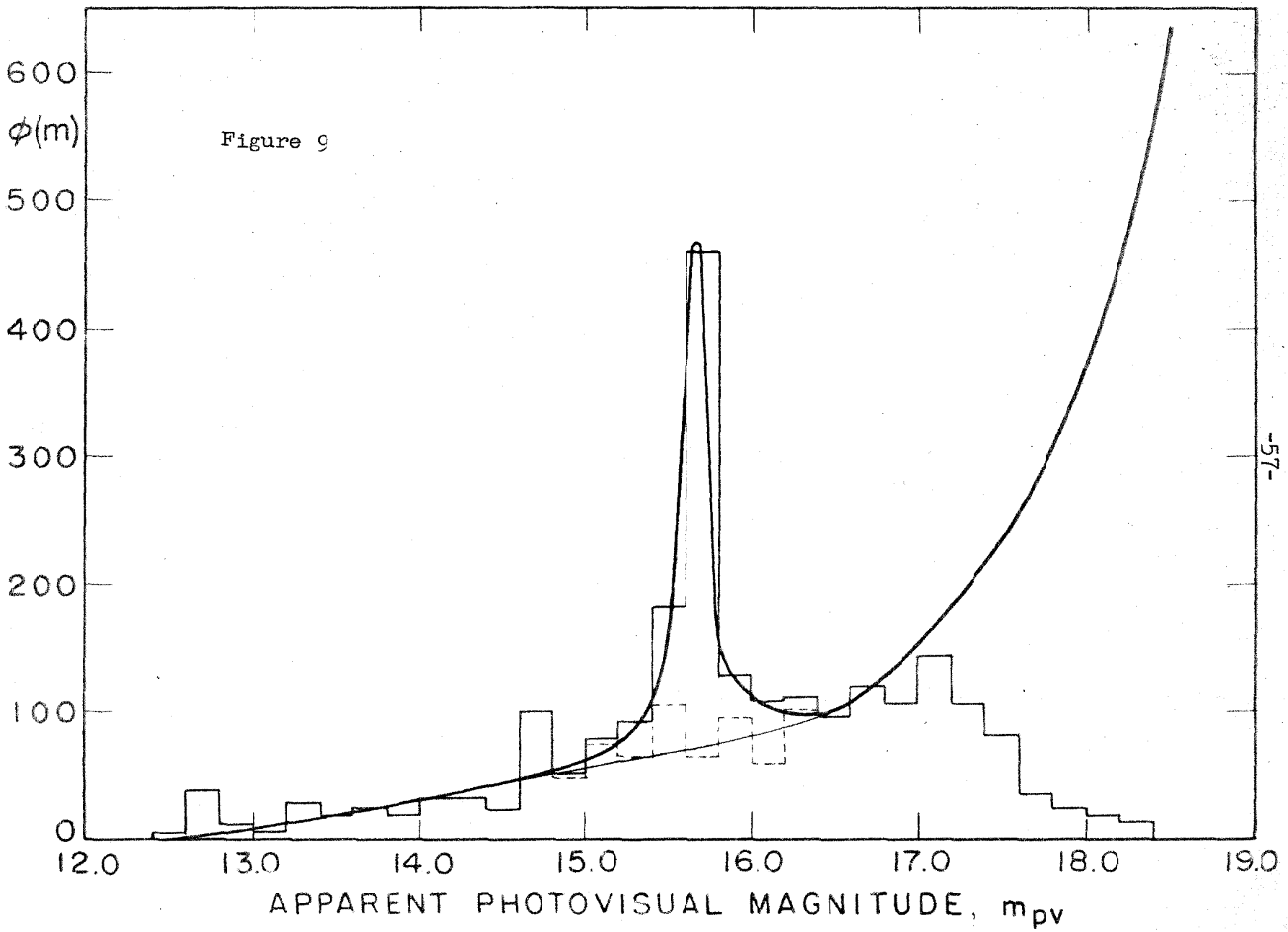
600
φ(m)
500
400
300
200
100
0
12.0
13.0
14.0
15.0
16.0
17.0
18.0
19.0
APPARENT PHOTOVISUAL MAGNITUDE, m_{pv}

Figure 9

Table 8

The Luminosity Function for M3

M	$\varphi(M_{pv})$*	N(M+0.1)	$\varphi(M_{pg})$*	N(M+0.1)	$\varphi(M_{Bol})$	N(M+.1)†
-4.0						
-3.8					2	2
-3.6					5	7
-3.4					8	15
-3.2					11	26
-3.0	1	1			14	40
-2.8	4	5			17	57
-2.6	8	13			20	77
-2.4	14	27			24	101
-2.2	17	44			28	129
-2.0	21	65			32	161
-1.8	26	91			35	196
-1.6	31	122			39	235
-1.4	35	157	4	4	43	278
-1.2	40	197	13	17	47	325
-1.0	45	242	20	37	51	376
-0.8	51	293	27	64	55	431
-0.6	59	352	34	98	60	491
-0.4	76	428	40	138	64	555
-0.2	120	548	80	218	69	624
0.0	420	968	311	529	75	699

Table 8 (Cont'd)

M	$\varphi(M_{pv})$*	N(M+0.1)	$\varphi(M_{pg})$*	N(M+0.1)	$\varphi(M_{Bol})$	N(M+1) ±
0.2	145	1113	261	790	81	780
0.4	111	1224	101	891	89	869
0.6	101	1325	74	965	98	967
0.8	101	1426	74	1039	110	1077
1.0	111	1537	78	1117	130	1207
1.2	131	1668	86	1203	159	1366
1.4	157	1825	95	1298	188	1554
1.6	183	2008	107	1405	226	1780
1.8	223	2231	125	1530	272	2052
2.0	270	2501	150	1680	325	2377
2.2	326	2827	180	1860	390	2767
2.4	402	3229	216	2076	465	3232
2.6	481	3710	261	2337	555	3787
2.8	586	4296	318	2655	647	4434
3.0	708	5004	390	3045	793	5227
3.2	871	5875	483	3528	940	6167
3.4	1072	6947	620	4148	1107	7274
3.6	1297	8244	809	4957	1320	8594
3.8	1567	9811	1020	5977	1580	10174
4.0	1786	11597	1300	7277	1820	11994
4.2	1972	13569	1556	8833	2020	14014
4.4	2138	15707	1760	10593	2180	16194
4.6	2291	17998	1940	12533	2330	18524

Table 8 (Cont'd)

M	$\varphi(M_{pv})$*	N(M+0.1)	$\varphi(M_{pg})$*	N(M+0.1)	$\varphi M_{(Bol)}$	N(M+.1) ∓
4.8	2427	20425	2110	14643	2460	20984
5.0	2523	22948	2256	16899	2550	23534
5.2	2570	25518	2376	19275	2600	26134
5.4	2624	28142	2470	21745	2620	28754
5.6	2618	30760	2540	24285	2594	31348
5.8	2570	33330	2580	26865	2524	33872
6.0	2489	35819	2605	29470	2420	36292
6.2	2355	38174	2612	32082	2268	38560
6.4	2188	40362	2586	34668	2060	40620
6.6	1959	42321	2540	37208	1775	42395
6.8	1726	44047	2450	39658		
7.0			2335	41993		
7.2			2200	44193		
7.4			2038	46231		
7.6			1840	48071		

* Includes horizontal branch

∓ Does not include horizontal branch

the subgiant and transition sequence of globular clusters (equation 34 Chapter 3). The relation fails fainter than $M_{Bol} = +4.0$ where the steep rise of $\varphi(M)$ is halted and the function, after passing through a maximum at $M_{Bol} = +5.5$ decreases for as far as the data can be carried. The exact form of the decrease in $\varphi(M)$ beyond $M_{Bol} = +5.5$ is uncertain due to the uncertainty in the value for the limiting magnitude of the last plate of Table 7. Since $m_{pv} = 22.5$ is likely to be a conservative value (too bright), the decrease in $\varphi(M)$ beyond $M_{pv} = +5.5$ is probably even more pronounced than shown in Figure 10. The existence of a negative slope to $\varphi(M)$ fainter than $M_v = +5.5$ is <u>therefore beyond doubt</u> but its quantative aspects are known only to the certainty which can be put in the limiting magnitude of PH-385-B.

2.3 The Application of $\varphi(M)$ to M3 and Other Stellar systems. Differences Between Globular Clustersand Elliptical Nebulae.

The data of Table 8 give the luminosity function for a globular cluster to adequately faint magnitudes so as to include all stars which contribute appreciably to the total light. Is this $\varphi(M)$ typical of all aggregates now classed as type II objects? The answer to this question can only come from a study of certain integral properties which may be inferred from a knowledge of

$\varphi(M)$. Several of these properties are discussed in this section.

Knowledge of $\varphi(M)$ permits an evaluation of the absolute magnitude of the cluster. By definition

$$M_{pv} = -2.5 \log \sum_{M_i=-\infty}^{+\infty} 10^{-0.4\, M_i}\ \varphi(M_{pvi}) \qquad (14)$$

where $M_{i+1} = M_i + 0.2$

The quanity $10^{-0.4\, M_i}\ \varphi(M_i)$ gives the contribution to the total light from stars in a range of magnitude M_i -0.1 to M_i +0.1. Table 9 tabulates the summation of equation (14) and shows how rapidly the weighting function $10^{-0.4 M_i}$ quenches the contribution of stars fainter than $M_i = +4$. Although the number of stars fainter than $M_i = +4$ becomes quite large, their contribution to the total light is almost negligible due to the rapid approach to zero of $10^{-0.4\, M_i}$. Ninety per cent of the photovisual light of M3 comes from stars brighter than $M_{pv} = 3.6$. The summation of the data of Table 8 by equation (14) gives $M_{pg} = -8.09$ for M3. The agreement with Christie's measured magnitude of $M_{pg} = -8.42$, ($m_{pg} = 7.21$, $m - M = 15.63$ from Chapter 1) shows

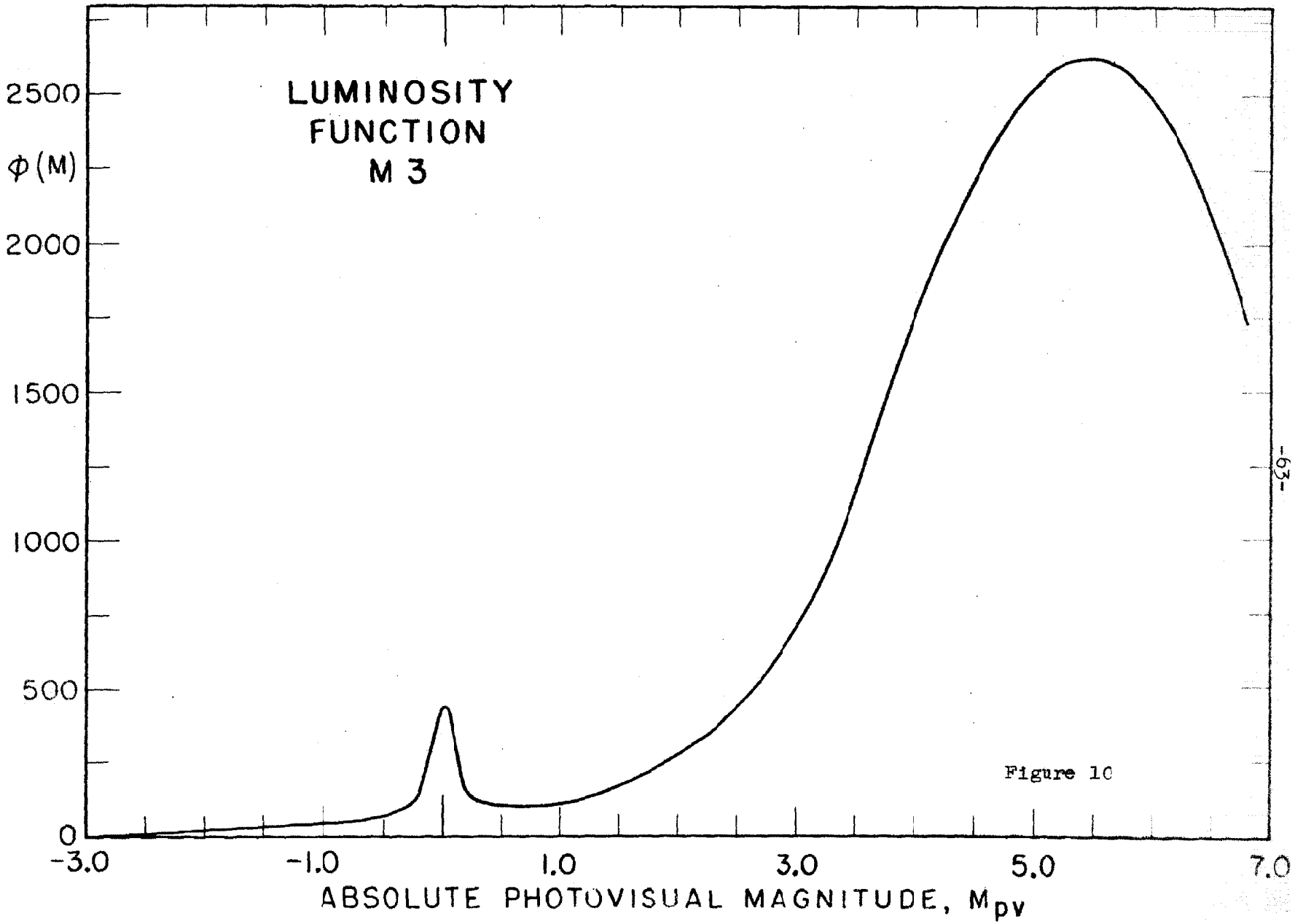
LUMINOSITY
FUNCTION
M 3
Φ(M)
2500
2000
1500
1000
500
0
-3.0
-1.0
1.0
3.0
5.0
7.0
ABSOLUTE PHOTOVISUAL MAGNITUDE, Mpv

Figure 10

that the $\varphi(M)$ derived in this investigation is essentially correct. This independent check of Table 8 indicates that the counting and magnitude errors entering the derivation of $\varphi(M)$ are small.

Table 8 shows that nearly all the light of M3 comes from stars brighter than $M_{pv} = 5.0$. This is not true of the contribution to the total mass. The mass of an aggregate with a luminosity function $\varphi(M)$ in which a mass-luminosity law $\mathcal{M}_i = f(L_i)$ operates is given by

$$\mathcal{M}_t = \sum_{L_i=-\infty}^{+\infty} f(L_i)\ \varphi(L_i) \qquad (15)$$

Unless the mass is a steep function of L_i, as for example the weighting function of equation (14), the large contributions to the total mass will come where $\varphi(L_i)$ is large, that is from the faint stars. Since $\mathcal{M}_i \propto L^{1/3}$ from Kuiper's mass-luminosity law[4], most of the mass of the aggregate comes from stars fainter than M = +7. This is the region where direct knowledge of the type II $\varphi(M)$ is unavailable and will be unavailable for many years to come. If some estimate of the total mass of M3 is to be made, an estimate of the value of $\varphi(M)$ for $M > +7$ must

Table 9

Summation of $\sum_{M_i = -3.0}^{M} 10^{-0.4\, M_i}\, \varphi(M_{pvi})$

M_i	$10^{-0.4\, M_i}\varphi(M)$	Fractional Light †	M_i	$10^{-0.4\, M_i}\varphi(M)$	Fractional Light †
-3.0	15.8	.005	2.6	43.9	.825
-2.6	87.6	.047	3.0	44.6	.852
-2.2	129	.124	3.4	46.9	.880
-1.8	136	.204	3.8	47.4	.908
-1.4	127	.283	4.2	41.2	.934
-1.0	113	.353	4.6	33.1	.955
-0.6	102	.416	5.0	25.2	.970
-0.2	144	.492	5.4	18.2	.982
+0.2	120	.654	5.8	12.3	.990
0.6	58.2	.694	6.2	7.8	.996
1.0	44.2	.722	6.6	4.4	.999
1.4	43.0	.748			
1.8	42.5	.773			
2.2	43.0	.799			

† This col. gives the fraction of the total light contributed by stars M_i and brighter

be had. Knowledge of $\varphi(M)$ fainter than M = +7 is available for the solar neighborhood from the work of Van Rhijn[5], Seares[6], Kuiper[7], Luyten[8], McCuskey[9] and others. As a first approximation, one might assume that the $\varphi(M)$ in the solar neighborhood is identical with $\varphi(M)$ in M3 fainter than M = +7. This assumption has been made in Figure 11. Its only justification is heuristic. If Figure 11 fainter than $M_{pg} = +7$ is adopted and if Kuiper's empirical mass-luminosity function[4] is valid, equation (15) gives

$$M_t = 1.1 \times 10^5 \quad M_\odot$$

for the mass of M3.

Is this reasonable? An independent evaluation of the mass of the globular cluster M92 has recently been made by O. C. Wilson[10] from the dynamical properties of a stellar aggregate assumed to be in statistical equilibrium. In such an aggregate the virial theorem gives a relation between the velocity dispersion of the individual system members and the total mass. Wilson's measurements of the radial velocities of the individual cluster stars of M92 gives $M_t = 5.6 \times 10^5 M_\odot$. The cluster M92 has an absolute magnitude of $M_{pg} = -7.82$ according to Christie's observation[3] of $m_{pg} = 7.30$ and the modulus[11] m - M = 15.12. M92 and M3 therefore seem to be quite

comparable objects. If it is assumed that the true mass of M3 is 5.6×10^5 M ⊙, the "extrapolated luminosity function" mass of 1.1×10^5 for M3 is a factor 5 too small. This result shows that the extrapolation of $\varphi(M)$ for M3 with the Van Rhijn function is incorrect. The Van Rhijn function is valid for the volume of space in the immediate neighborhood of the sun. The most recent investigations of Morgan, Sharpless, and Osterbrock show[12] that the solar neighborhood is in, or near one of the spiral arms of the galactic system. Hence the Van Rhijn function refers to a mixture of type I (spiral arm) and type II populations with the type I probably dominant. The discrepancy in the dynamical mass and "extrapolated $\varphi(M)$" mass of M3 by a factor of 5 then leads to the conclusion that the number of dwarf stars in globular cluster population fainter than $M_v = +7$ exceeds the number in a predominately type I population by a factor of about 10. [Since the average mass of stars in the magnitude interval here considered (M = +7 to +20) is about .5 M ⊙, a mass discrepancy by a factor 5 gives a discrepancy in total numbers by a factor of 10]. Since the evolutionary changes in stars fainter than M = +7 are entirely negligible in the time interval of 5×10^9 years (the age of M3 and M92 established in Chapter 3) this greater number of dwarf stars in the

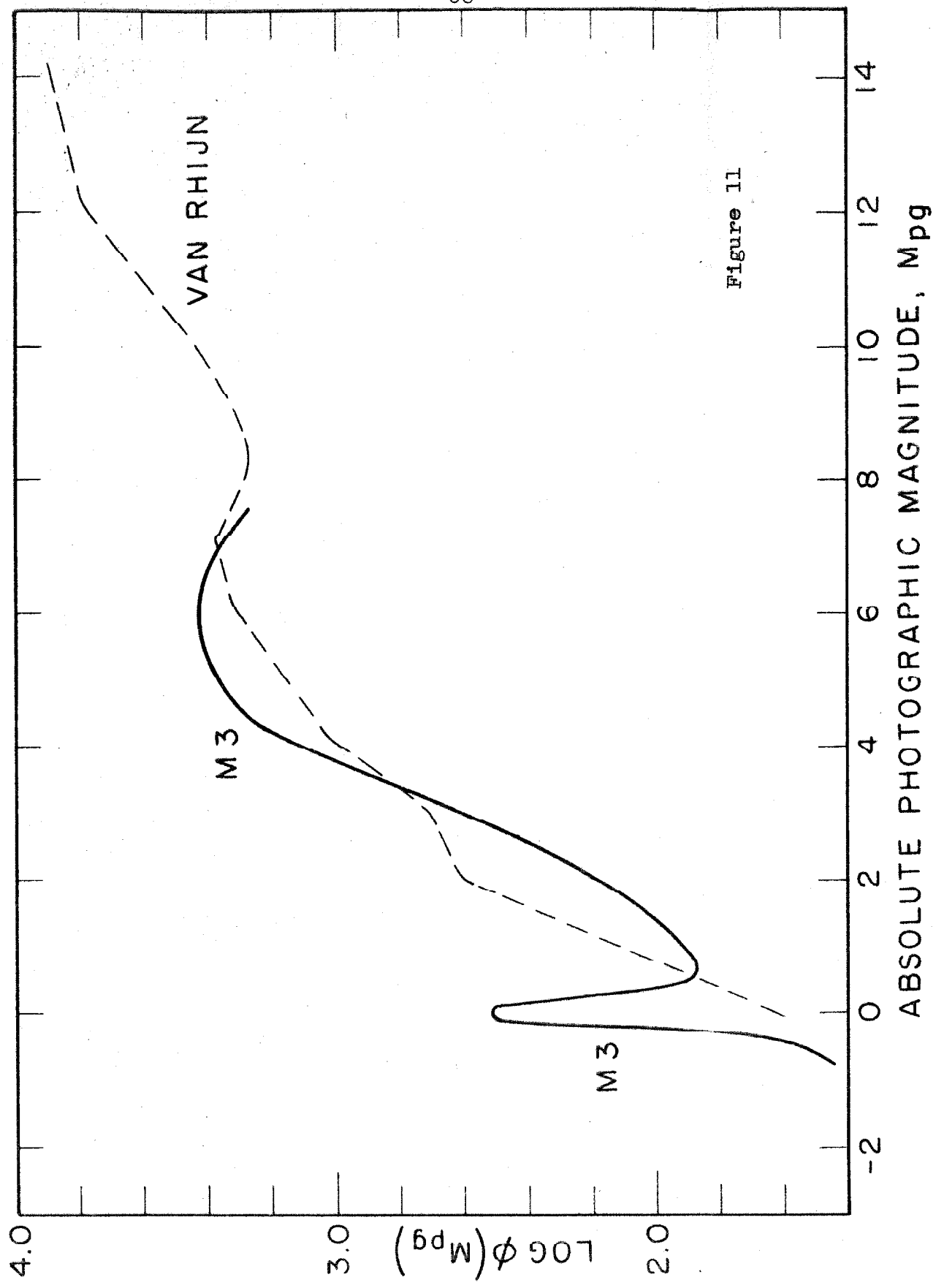
VAN RHIJN
M3
M3
LOG Φ(Mpg)
4.0
3.0
2.0
-2
0
2
4
6
8
10
12
14
ABSOLUTE PHOTOGRAPHIC MAGNITUDE, Mpg

Figure 11

type II population is of cosmogonic rather than evolutionary origin. Therefore the $\varphi(M)$ for M3 is not at all typical of the type I spiral arm aggregate for the faint stars. Furthermore, Figure 11 shows that it is not similar to the Van Rhijn function in its bright portion either.

However, is the M3 $\varphi(M)$ typical of other systems now classed as type II objects such as elliptical nebulae? If the luminosity functions for globular clusters and for elliptical nebulae were identical, the mass to light ratios for these two classes of objects should be the same. Adopting O. C. Wilson's mass of 5.6×10^5 M ⊙ for M3 and an absolute magnitude of $M_{pg} = -8.1$, the mass to light ratio (in units of the solar values) is 2.7. The object among the extra-galactic nebulae whose mass is best known is M31. Although M31 is not an E nebula, Holmberg has shown that 5/6 of the total light of M31 comes from the nuclear region which is of type II population. Furthermore nearly all the mass is in this region. Hence the M/L ratio in M31 will simulate closely that of an E nebula. The mass of M31, obtained from rotational velocities measured by N. U. Mayall[13] and from the new distance modulus of m - M = 23.9 by Baade[14], is $M_t = 4 \times 10^{11}$ M ⊙. The total apparent magnitude of M31, determined by A. E. Whitford[15] in

1936 with the photocell, is m_{pg} +4.5. This corresponds to an absolute photographic magnitude of +4.5 - 23.9 = -19.4. The corresponding mass to light ratio is 58. If Holmberg's factor 5/6 for the fraction of the total light contributed by the nucleus is correct, the mass to light ratio for an elliptical nebulae should be M/L = (6/5) × (58) = 70. This is nearly 30 times that for M3. This large M/L points to an even larger population of dwarf stars in elliptical nebulae than in globular clusters and clearly indicates that the $\varphi(M)$ for M3 is not typical of elliptical nebulae.

A much stronger argument may be advanced for showing that globular clusters and elliptical nebulae are not scale models for one another. The energy distribution with wave length of a system of stars is formed from the properly weighted individual energy distribution curves for each member star. Let $\mathcal{E}_\lambda(T_i)$ be the energy emitted per second per square cm. of emitting surface for a star at temperature T_i. For a black body, $\mathcal{E}_\lambda$ is given by Planck's function. The total energy emitted by star i at temperature T_i per second at wave length λ is $\mathcal{E}_\lambda(T_i)\ 4\pi R_i^2$. Let there be $\varphi(T_i)$ stars of temperature T_i in the stellar system considered. The total energy radiated per second by the entire system at wave length λ will be

$$E_\lambda = 4\pi \sum_{T_i} \varepsilon_\lambda (T_i) R_i^2 (T_i) \varphi(T_i) \qquad (16)$$

If there is a well defined Hertzsprung-Russell diagram for the aggregate, $\varphi(T_i)$ is uniquely related to the luminosity function $\varphi(M)$ since there exists a function f such that $T_i = f(M)$. Similarly the existence of sequences in the H-R diagram assures that $R_i = g(T_i)$. Hence, for two stellar aggregates with the same luminosity function and with identical sequences in the H-R diagram, equation 16 shows that the energy distribution curves must be identical. Observations by Stebbins and Whitford [16,17] show that this is not the case for globular clusters compared with elliptical nebulae. The photoelectric measurements of M32 at six wave lengths, converted from differential color measurements to relative intensities by reference to E. Pettit's solar energy distribution curve[18], is shown in Figure 12. Also shown in Figure 12 is the mean intensity curve for four globular clusters measured by Stebbins and Whitford reduced in the same manner. These measurements for the clusters M2, M13, M15 and M92 were reported by Stebbins in his George Darwin Lecture of 1950[17]. The difference shown in

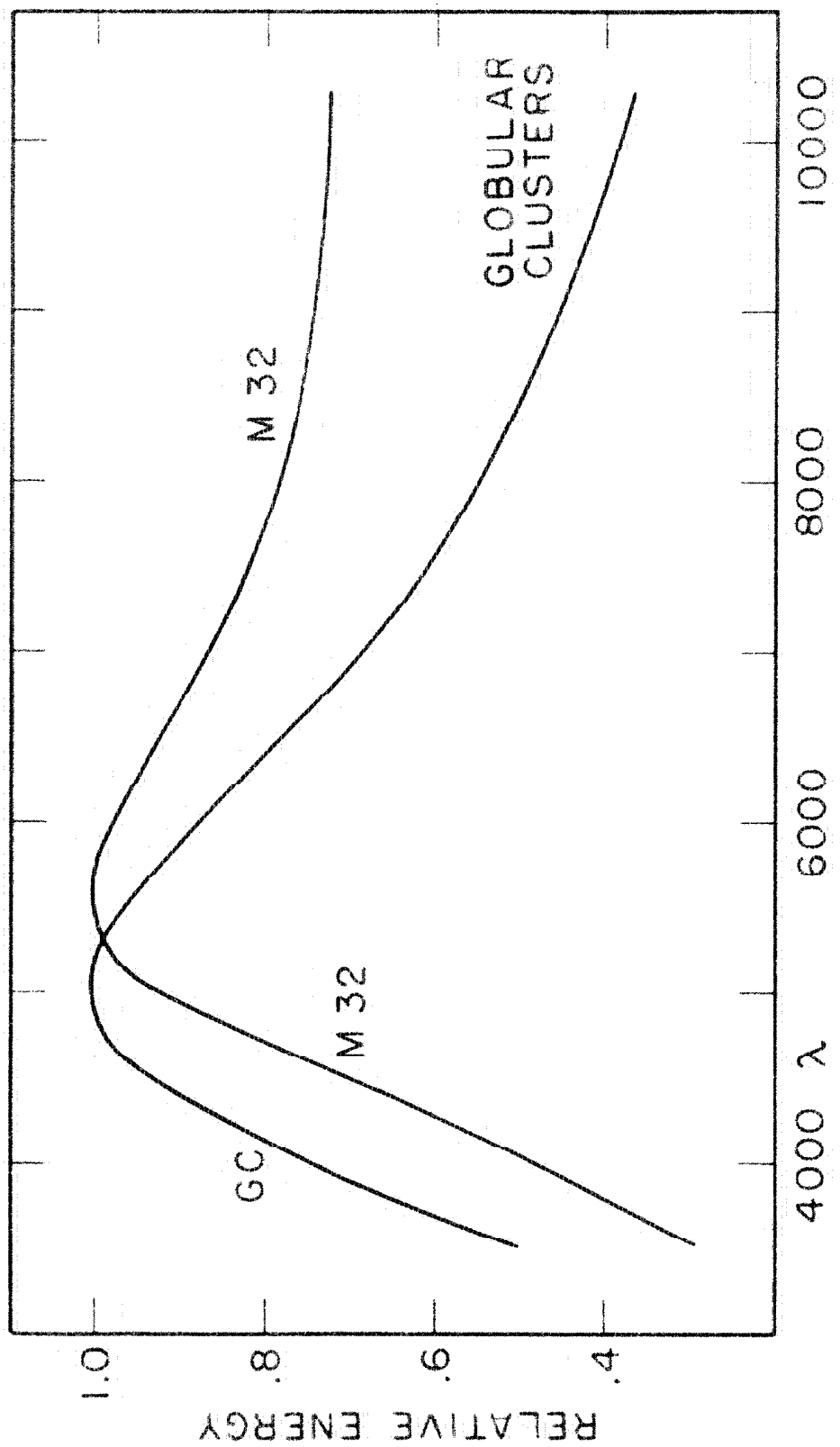
RELATIVE ENERGY
1.0
.8
.6
.4
4000 λ
6000
8000
10000
GC
M 32
M 32
GLOBULAR CLUSTERS

Figure 12

Figure 12 between a typical E nebula and typical unobscured globular clusters is striking and can be explained by two possibilities. (1) The sequences in the H-R diagrams for E nebulae and globular clusters are identical but the distribution of stars along these sequences, $[\varphi(M)]$, differs: or (2) The H-R diagrams for the two types of objects are different so that the ε_λ and the weighting function R^2 (T_1) differ. If alternative 2 is correct, Baade's identification[19] of the globular cluster population with that of the elliptical nebulae and the nucleus of M31 upon his resolution of M31 is thrown open to question. However Baade's plates of M31 show resolution of the individual globular clusters into stars at the same limiting magnitude for which the sheet of the underlying type II population just becomes visible[20]. This observation proves that the brightest stars in the elliptical nebulae have the same absolute magnitude as the brightest stars in the globular clusters. This however proves nothing as to the strict identity of the sequences in both color and magnitude in the H-R diagram for E nebulae and globular clusters. At present the solution of the discrepancy shown in Figure 12 is an open question which can only be solved if an H-R diagram for an elliptical nebula can be obtained. There

is hope in this direction since the two Sculptor type systems in Leo[21] and the new system in Draco[22] found by A. G. Wilson from 48-inch Schmidt Sky Survey plates are near enough to reach $M_{pv} = +2$ with the 200-inch and are loose enough to be able to measure the individual stars. Such a study will be important since these diagrams will provide the decision between alternative (1) and (2).

The situation is further complicated by recent observations by O. C. Wilson[23] of the integrated spectrum of M92 and by R. Minkowski[24] of the integrated spectrum of M32. The M92 spectrum shows extremely weak metal lines and corresponds well with the peculiar spectra of the brightest stars of the cluster obtained by O. C. Wilson and I. S. Bowen[25]. The M32 spectrum shows the normal type I spectrum devoid of the extreme type II characteristics of M92. This fact indicates that the types of stars comprising M92 and M32 are quite different (possibly due to chemical composition differences). If both types of objects are classed as type II population, as is current practice, it is clear that there must be a subdivision within this population grouping.

Is there evidence for such a subdivision in our own galaxy? Perhaps a distinction should be made

in the galactic system between three groups of objects; (1) the objects of the spiral arm population (type I), (2) the non-spiral arm population of the disc of our galaxy, and (3) the objects which populate the halo of the galactic system. Most globular clusters are of the halo population while most galactic clusters are spiral arm population I. There are however galactic clusters in the disc which are not population I such as M67 and M11. The color-magnitude diagrams for these are not like the usual galactic clusters but resemble somewhat those of globular clusters. They are similar but not identical. A partly completed investigation of the color-magnitude diagram of M67 by H. L. Johnson and the present author indicates that the M67 sequences are redder than those of M3 by 0.3 magnitudes the cause of which is not selective absorption but is intrinsic in the sequences. M67 and M11, which appears to be similar, might therefore be classed as disc population II (since they certainly are not spiral arm aggregates but they are located in the galactic plane) while M3 and most other globular clusters may be classed as halo population II objects. The sense of the sequence differences between M 3 and M67 is that required to explain the differences shown in Figure 12, if the E nebulae are

classed as predominantly disc population II.

One striking example of a disc population globular cluster is NGC 6522 which is embedded in the nuclear star clouds of our galaxy. If this cluster were typical of M2, M13, M15 and M92 of Figure 12, and if the nuclear star clouds of our galaxy are typical of the elliptical nebulae stars, there should be a difference in the color of NGC 6522 and the surrounding star field. However differential color measurements with photoelectric equipment by Stebbins and Whitford[26] showed no difference in color between NGC 6522 and the nuclear stars amounting to more than 0.01 magnitudes. This is an extremely significant result in view of Figure 12. A difference of 0.31 magnitudes is expected if the energy distribution curves of the two aggregates were like those of Figure 12. The observational result shows that NGC 6522 and the aggregate of nuclear stars have similar energy distribution curves. NGC 6522, from its position in the nucleus of our galactic system, is to be classed as a disc population II. The dichotomy indicated by Figure 12, M67 and M11, NGC 6522 and the nuclear stars may support the suggestion for a difference in a disc and halo population II.

It will be of interest to obtain the integrated spectrum of NGC 6522 to see if it shows the weak line

characteristics of M92 or the normal charcteristics of M32. The prediction from the above hypothesis is that the spectrum of NGC 6522 will be like that of M32 rather than M92, reflecting a disc population rather than a halo population II.

2.4 The Projected Radial Density Distribution Function $\rho(m, r)$ in M3

Probably no aspect of globular clusters has been more completely studied than that concerning the three dimensional density distribution of the cluster stars. The only reason for now reopening the subject is the availability of new observational data from plates taken with the 200-inch telescope. The fine definition and large scale of these plates are factors of some importance for obtaining accurate counts. Furthermore, the new data extend to faint magnitudes permitting studies of segregation of the bright from the faint stars.

The problem of obtaining the three-dimensional density function $\Phi(r)$ from the projected function, $\rho(x)$, has been solved by von Zeipel[27] and independently by Plummer[28] by a different method. In both methods, the datum of observation is the areal density obtained from counts on photographic plates. The well known integral equation connecting $\Phi(r)$ and $\rho(x)$,

first obtained by von Zeipel is

$$\rho(x) = 2 \int_x^R \frac{r \, \Phi(r) \, dr}{(r^2 - x^2)^{1/2}} \qquad (17)$$

where R is the limiting radius of a spherical configuration. Von Zeipel has shown that equation 17 may be reduced to Abel's integral equation and hence $\Phi(r)$ formally obtained but the solution is not of great practical use since it requires differentiation of the observational data, $\rho(x)$, and such differentiation can give spurious results unless the empirical data are of the highest accuracy. As emphasized by many people and most recently by Chandrasekhar and Münch[29], it is better to assume a distribution function with adjustable parameters for $\Phi(r)$ and to determine the parameters with equation 17 by fitting to the empirical $\rho(x)$.

Plummer, in his paper[28] of 1911 argues, by analogy with a gas sphere in hydrostatic equilibrium, that stars in a globular cluster should follow a polytropic density law given by the solutions to Emden's fundamental differential equation governing such systems. Plummer adopted the solution with polytropic index 5 and found that $\Phi(r)$ would be given by

$$\Phi(r) = \frac{B}{(a^2 + r^2)^{5/2}} \qquad (18)$$

where a and B are constants. In what follows, this function will be known as Plummer's law. If this law is valid, the cluster is infinite in extent but the total number of stars contained is finite since

$$N = 4\pi B \int_0^\infty \frac{r^2\, dr}{(a^2 + r^2)^{5/2}} = \frac{4\pi B}{3 a^2} \qquad (19)$$

Equation (18) substituted in (17) and integrated using (19) gives the areal density as

$$\rho(x) = \frac{Na^2}{(a^2 + x^2)^2} = \frac{\rho(0)}{\left(\frac{x^2}{a^2} + 1\right)^2} \qquad (20)$$

How closely does this agree with the empirical data? The counts used in section 2.2 to obtain the luminosity function were made in circular rings concentric with the nucleus. From these data, the number of stars, $\rho(m, r)$, brighter than apparent magnitude m per square minute of arc at a distance r from the center, was obtained. The data are given in Table 10 and shown in Figure 13 where they have been smoothed.

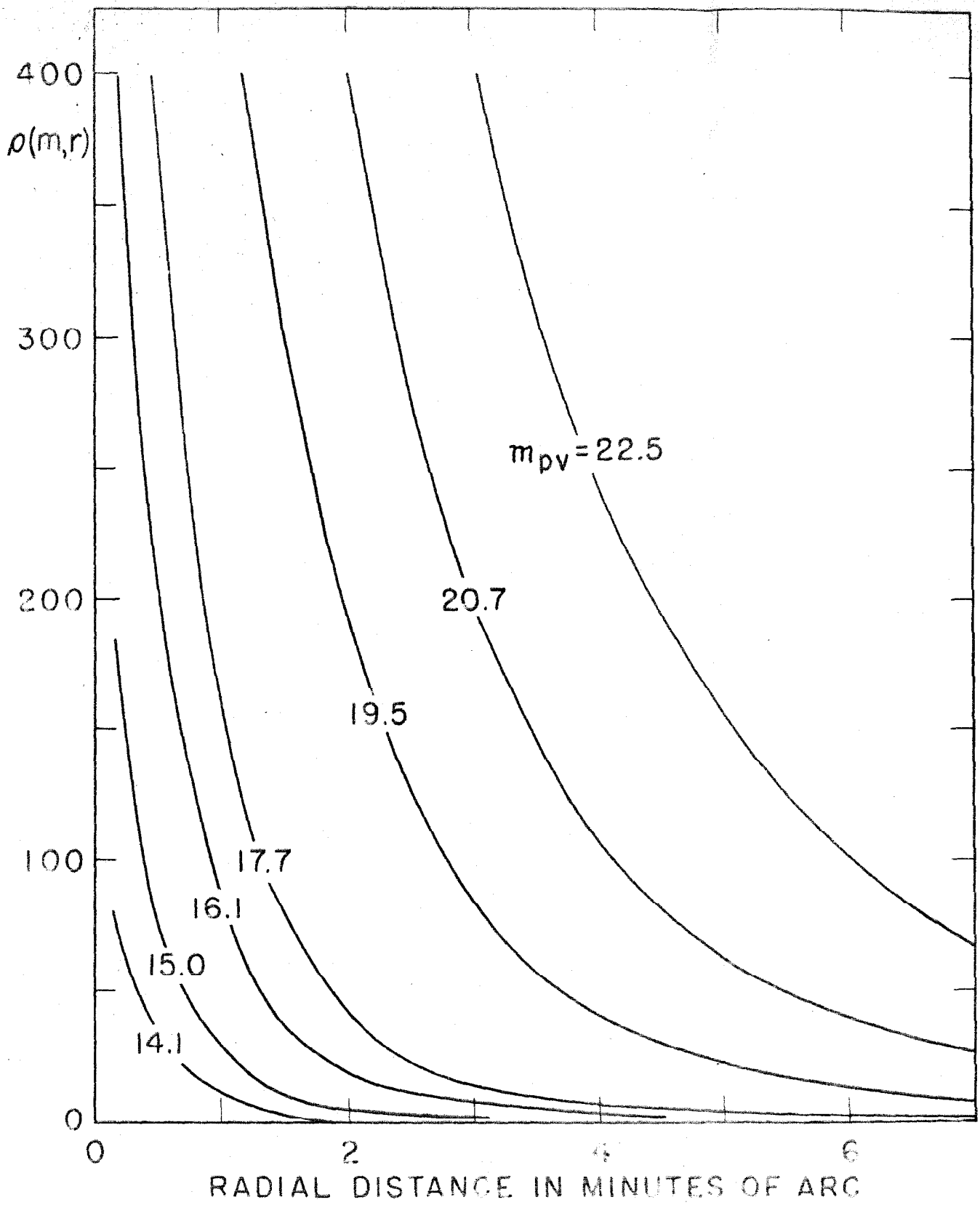
400
ρ(m,r)
300
200
100
0
0
2
4
6
RADIAL DISTANCE IN MINUTES OF ARC
m_pv = 22.5
20.7
19.5
17.7
16.1
15.0
14.1

Figure 13

Table 10

Areal Density $\rho(m, r)$. Unit is Number of Stars per Sq. Minute

r \ m_{pv}	14.1	15.0	16.1	16.9	17.7	19.5	20.1	20.7	21.5	22.5
7"5	89.47	184.9	405.6							
22"5	44.04	120.9	256.5	289.6						
45"	21.47	46.45	136.4	182.5	241.2					
1'15"	6.39	17.46	52.92	74.41	111.6					
1'45"	2.34	6.23	26.82	38.79	53.87		407.7	439.4		
2'15"	1.81	3.77	13.26	21.07	29.96	155.7	259.8	326.3	527.8	610.8
2'45"	1.19	2.96	10.00	13.50	16.82	97.17	174.2	237.2	402.2	471.2
3'15"		1.50	5.11	7.92	12.17	74.32	118.5	171.2	277.2	355.7
3'45"		0.38	3.20	4.68	7.71	52.08	72.24	120.0	206.9	275.3
4'15"		0.43	2.38	3.89	6.16	34.93	58.86	95.57	161.5	209.2
4'45"			2.12	3.27	4.22	26.12	37.86	73.65	124.7	179.5
5'15"				2.34	3.53	19.75	28.97	55.61	92.38	149.2
5'45"					2.96	17.89	25.72	45.85	77.49	112.8
6'15"						12.12	21.59	37.05	60.07	92.64
6'45"						8.52	14.50	29.13	51.17	74.84
7'15"						6.06	12.57	22.16	38.22	52.73
7'45"						6.58	11.12	19.06	32.33	50.05
8'15"							7.06	15.60	28.94	41.66

Inspection of Figure 13 shows that segregation exists between the bright and faint members of the cluster. The faint stars are much less concentrated toward the nucleus than the bright ones. The effect is pronounced and easily seen by comparing the shape of $\rho(22.5, r)$ with that of say $\rho(16.1, r)$. It is significant (see section 3.3 of Chapter 3) that the shape of the $\rho(m, r)$ curves from $m_{pv} = 14.1$ to about 17.7 are nearly identical, while fainter curves show progressively different forms. For these brighter curves, the relation $\rho(m_1, r) = c\ \rho(m_2, r)$ is a good approximation. This is not true for the curves fainter than $m_{pv} = 19.5$. Chapter 3 discusses the significance of this segregation in terms of mass ratios.

If Plummer's density law is valid, equation 20 should fit the data. Table 11 compares the values of $\rho(x)$ computed from equation 20 with the observed $\rho(x)$ read from the smoothed curves in Figure 13 and shows that equation 20 fits the data exceedingly well for the faint stars. All differences, $\rho(x)_o - \rho(x)_c$, for stars fainter than $m_{pv} = 19.5$ are within the errors of observation. For the stars brighter than 17.7, Plummer's law predicts too large a value for $\rho(x)$ for small x and too small a value for $\rho(x)$ at large x. These differences

Table 11

Comparison of $\rho(x)$ Computed from Equation 20 with $\rho(x)$ Observed

	m_{pv} = 15.0		m_{pv} = 17.7		m_{pv} = 19.5		m_{pv} = 22.5	
x'	$\rho(x)_c$	$\rho(x)_o$	$\rho(x)_c$	$\rho(x)_o$	$\rho(x)_c$	$\rho(x)_o$	$\rho(x)_c$	$\rho(x)_o$
.15	164.0	185						
.25	147	148						
.4	115	100						
.5	94	77	374	374				
.75	53	46	276	245				
1	29	29	191	157				
1.5	9.5	11	88	80	306	305		
2	3.76	4	42	42	200	193	375	402
2.5			21	22	129	127	281	280
3			12	13	84	84	207	199
3.5			6.9	9	56	57	152	146
4			4.3	7	38	40	112	107
4.5					26	30	83	80
5					19	22	63	62
5.5					14	17	47	49
6					10	13	36	39
6.5					7.5	10	28	32
7					5.8	7	22	27

are larger than the errors of observation and show real inconsistencies with equation 20. This departure from Plummer's law of the bright stars is similar to that found by G. L. Camm[30] using data obtained from small scale plates by W. Lohmann[31]. Camm's law, derived for an equilibrium configuration whose gravitational potential is given only by the member stars, may fit the data for the bright stars better than equation 20.

It is of interest to compare equation 20 with Hubble's empirical relation[32] in E nebulae. Hubble's extensive measurements show that an equation of the form

$$I(x) = \frac{I(0)}{\left(\frac{X}{a} + 1\right)^2} \qquad (21)$$

fits the observed intensity decrement for elliptical galaxies well. To compare equation 21 with 20 some assumption must be made about the relation between the areal density, $\rho(x)$, and the intensity function $I(x)$. There is no a priori reason to suppose that the form of the two functions differ. Furthermore, unpublished observations of M3 with photoelectric equipment by Arthur A. Hoag at the Naval Observatory show almost exact agreement of his $I(x)$ with the $\rho(x)$ function

shown in Figure 13 for m_{pv} brighter than 17.7. Hence equation 21 for E nebulae may be written

$$\rho(x) = \frac{\rho(0)}{\left(\frac{x}{a} + 1\right)^2} \qquad (22)$$

Comparison of equation 22 with equation 20 shows that the density function is much steeper in globular clusters than in elliptical nebulae. As $x \to \infty$ the E nebulae fade as x^{-2} whereas the globular clusters go as x^{-4}. This again emphasizes that elliptical nebulae and globular clusters are not mere scale models of one another but differ in a more basic way.

A complete analysis of the data of Table 10 to obtain mass ratios has not been attempted. When similar data for M13 and M92 have been accumulated, a discussion of the complete material will be profitable in an effort to obtain a mass-luminosity relation for type II stars. Although the validity of such arguments have been questioned by many people due to the necessary assumption that the age of the cluster is significantly longer that the relaxation time in the region of the cluster analyzed, such an attempt to derive mass-ratios seems important to obtain any information possible on the mass-luminosity law for type II stars.

References for Chapter 2

1. W. Baade in a footnote, Ap.J., 100, 137, 1944
2. J. P. Kuiper, Ap.J., 88, 429, 1938
3. W. H. Christie, Ap.J., 91, 8, 1940
4. J. P. Kuiper, Ap.J., 88, 472, 1938
5. P. J. van Rhijn, Groningen Pub. No. 47, 1936
6. F. H. Seares, Ap.J., 59, 299, 1924
7. J. P. Kuiper, Ap.J., 95, 201, 1942
8. W. J. Luyten, Minnesota Pub. 2, No. 7, 1939
9. S. W. McCuskey, Pub. Obs. Univ. Mich. Vol 10, 67, 1951
10. O. C. Wilson, Private conversation
11. Arp, Baum and Sandage, A.J., 58, 4, 1953
12. Morgan, Sharpless, and Osterbrock, A.J., 57, 3, 1952
13. N. U. Mayall, Pub.Obs. Univ. Mich., 10, 19, 1951
14. W. Baade, Minutes of Meeting of Commission 28, I.A.U., Rome, Sept. 4-13, 1952
15. A. E. Whitford, Ap.J., 83, 424, 1936
16. Stebbins and Whitford, Ap.J., 108, 413, 1948
17. J. Stebbins, M.N., 110, 416, 1950
18. E. Pettit, Ap.J., 91, 172, 1940
19. W. Baade, Ap.J., 100, 137, 1944
20. W. Baade, Private conversation
21. A. G. Wilson and R. Harrington, P.A.S.P.,60, 118, 1950
22. A. G. Wilson, Unannounced discovery as of May 1953

23. O. C. Wilson, Private conversation

24. R. Minkowski, Private conversation

25. W. A. Baum, A.J., 57, 222, 1952

26. J. Stebbins and A. E. Whitford, Ap.J., 106, 235, 1947

28. H. C. Plummer, M.N., 71, 460, 1911

29. S. Chandrasekhar and G. Münch, Ap.J., 11, 142, 1950

30. G. L. Camm, M.N., 112, 155, 1952

32. E. P. Hubble, Ap.J., 71, 231, 1930

Figure Captions for Chapter 2

Figure 9. The luminosity function for the bright stars in M3. The histogram is based upon counts in Table 6 multiplied by the factor 3.5. The dotted histogram is that resulting from the exclusion of stars bluer than CI = 0.50 from the counts. The high peak at m_{pv} = 15.6 is due entirely to the stars on the horizontal sequence. Note the relative incompleteness of Table 6 fainter than m_{pv} = 17.0.

Figure 10. The total luminosity function for M3 to M_{pg} = +6.8 obtained from star counts in the cluster. The existence of the decrease fainter than M_{pv} = +5.5 is beyond doubt but its exact form is uncertain for observational reasons.

Figure 11. A comparison of the Van Rhijn luminosity function with that of M3. The conspiciuous differences at the bright end are evident. Arguments in the text show that the Van Rhijn function cannot be a valid extrapolation of the M3 data to magnitudes

fainter than +7. The suggested fit of this diagram is therefore incorrect.

Figure 12. A comparison of the energy distribution curves of four typical globular clusters and of M32. The great differences shown strongly suggest a dichotomy of type II systems.

Figure 13. The projected radial density curve for stars of different magnitude in M3. Note the greatly different shape of the $m_{pv} = 22.5$ curve compared with $m_{pv} = 17.7$ showing segregation of the bright and faint stars.

Chapter 3. An Evolutionary Theory for the Globular Cluster Color-Magnitude Diagram

3.1 Introduction

The data of Chapters 1 and 2 show the unique and peculiar characteristics of type II aggregates as compared with normal type I systems. In particular, stars on the main sequence of the color-magnitude diagram brighter than $M_{Bol} = +3.5$ are virtually absent. All stars brighter than this absolute magnitude are in the subgiant and giant regions of the H-R plane or on the horizontal branch situated in the Hertszprung gap. The portion of the diagram fainter than $M_V = +3.5$ appears to be normal, since all stars in this magnitude range are on the main sequence. Furthermore, there is no dust in globular clusters out of which new stars can be formed; hence all members of the cluster are likely to be the same age.

The explanation of these features by a single underlying principle, must be the goal of the theory of stellar structure. No complete theory is available at present. However the broad outline of an eventual detailed explanation of Figure 1 appears possible.

Work in the theory of stellar structure has succeeded in the past 30 years in explaining the main sequence of the H-R diagram with chemically homogeneous stellar models. Until fairly recently the giant and supergiant regions of the diagrams have been closed to detailed attack since homology transformations from main sequence models to giant models give central temperatures for the giants far too low for nuclear energy generation processes to operate. Öpik's initial suggestion[1] and Hoyle and Lyttleton's subsequent independent suggestion[2] that chemically inhomogeneous stellar models can have large radii and internal temperatures high enough for the nuclear processes to go have given rise, in recent years, to many papers on the problem of giant stars. It remains however to explain the existence of narrow-sequences in the giant region such as those of type I, luminosity class III stars and those of globular clusters. The ultimate aim of any theory must be for an explanation of the form of these sequences in terms of either a cosmogonic or an evolutionary process for the creation of the chemical inhomogeneities. The absence of the main sequence in M92 and its virtual absence in M3 brighter than $M_V = +3.5$ do suggest that evolution is occurring in these clusters taking stars from the main sequence into

the giant region as physical processes create changes in the deep interior. It is easy to see how stars which do not mix, can build up chemical inhomogeneities through the manufacture of helium out of hydrogen as they age. The evolution of such unmixed stars promises to explain the M3 color-magnitude diagram.

3.2 Details of the Evolutionary Process to $M_{Bol} = +2$

The evolution of a star from the time of its birth depends rather critically upon the nature of the processes occurring in its interior. Whether mixing does or does not occur is of primary importance in deciding if a star will remain on the main sequence or will move from this sequence in its evolutionary life. B. Strömgren has shown[3] that a chemically homogeneous star, completely mixing the products of the nuclear reactions in its interior, evolves nearly along the main sequence toward higher luminosities. Clearly such an evolutionary path cannot explain the globular cluster stars which are off the main sequence. However, from the work of Öpik, Hoyle and Lyttleton, and many others, models with a variation of molecular weight from interior to envelope are known to populate the giant region of the H-R diagram. It is

therefore suggestive that stars on the globular cluster subgiant and giant sequences can be explained by such non-mixed, chemically inhomogeneous models. Evolutionary tracks for such stars have recently been computed by Martin Schwarzschild and the present author[4] with a gravitationally contracting model introduced by Schwarzschild. The resulting scheme of evolution follows.

Stars at birth are assumed to be chemically homogeneous and hence on the main sequence with a convective core and a radiative envelope (Cowling's model). These stars, assumed not to mix between the energy producing interior and the hydrogen rich envelope, begin to age and start exhausting their hydrogen supply in the interior. The subsequent early stages of the evolution follow those computed by Schönberg and Chandrasekhar[5] with the core finally becoming exhausted of hydrogen and therefore isothermal. With no hydrogen remaining in the interior, the nuclear-energy production is confined to a shell between the exhausted core and the radiative envelope. This shell burns outward into the hydrogen rich envelope until 12 percent of the total mass of the star is contained within it. At this point the shell can no longer expand since, as Schönberg and Chandrasekhar have shown[5], an equilibrium configuration

with a radiative envelope and an isothermal core is not possible if the core contains more than 12 per cent of the total mass of the star. When this limiting model is reached, the core is assumed to contract under its own gravity giving rise to a large temperature gradient in what was once the isothermal region. This temperature gradient causes the entire structure of the star to alter so that the envelope greatly expands and the star rapidly moves away from the main sequence into the giant region of the H-R plane. A series of seven models in an evolutionary sequence were computed in the investigation quoted[4]. The conclusions drawn from these computations were[4]: "[The computed evolutionary tracks] suggest the following explanation for the Hertzsprung-Russell diagram for old stellar systems - such as globular clusters - in which all stars are presumably of the same age. The fainter stars of such a system will not yet have burned up 12 per cent of their mass and will therefore be on or near the main sequence. The brighter stars will have burned up more than 12 per cent of their mass and will therefore have moved to the right in the H-R diagram. [The computed evolutionary tracks further show that] the evolution [into the giant region] sets in rather sharply ------. Hence one should expect a fairly well

defined turn off point in the H-R diagram of these systems, as is indeed observed. The stars at the turn off point should then be identified with those which have just reached the Schönberg-Chandrasekhar limit, i.e., have just burned out 12 per cent of their mass."

Hence in an old stellar system the main sequence should be devoid of stars brighter than a certain luminosity - luminous stars originally on the main sequence having moved into the giant region. In contrast, stars which have not created chemical inhomogeneities will remain on the main sequence following B. Strömgren's evolutionary track[3]. (This may be the explanation for the few scattered stars in M3 on the main sequence brighter than $M_V = +3.5$.)

If the turnoff point from the main sequence in M3 and M92 is identified with the Schönberg-Chandrasekhar limit, this theory offers a means of computing the age of globular clusters. Stars now at $M_{Bol} = +3.5$ have converted 12 per cent of their hydrogen into helium. The computations of Schönberg and Chandrasekhar[5] concerning the first stages of the evolution show that these stars started their life from a point on the main sequence one magnitude fainter, or at $M_{Bol} = +4.5$. The age for M3 and M92 comes from the answer to the question: How

long has it taken for this 12 per cent mass conversion to occur? If the star were to remain at a constant luminosity, L, throughout the process, the time t to burn a percentage q_1 of the total mass is

$$t = \frac{.007\ q_1\ X_e\ M\ c^2}{L} \qquad (23)$$

where X_e is the fractional hydrogen abundance by weight in the envelope, c the velocity of light, q_1 the percentage of the total mass burned and M the total mass of the star. (It can be shown that $q_1\ X_e$ is a constant equal to .072 for the models considered). Since, however, L is not constant as q_1 varies from 0 to .12 but increases by 1 magnitude, equation 23 cannot be used. However, Schönberg and Chandrasekhar give the change of L with q_1 in Figure 3 of their paper[5] making the evaluation of equation 23 in finite steps possible, each step i being sufficiently small so the variation of L_i may be neglected. The time spent in step i is then

$$\delta t_i = \frac{.007\ X_e\ M\ c^2}{L_i}\ \delta q_i \qquad (24)$$

Reference 5, Figure 3 gives $L_i = f(\delta q_i)$. Since the data of Figure 1, Chapter 1 of this thesis show that the stars start their evolution at $M_{Bol} = +4.5$, the mass M in equation 24, to sufficient approximation, is M ⊙. Numerically equation 24 becomes

$$t = \sum_i \delta t_i = \sum_i \frac{6.243 \times 10^{10}}{L_i/L_\odot} \delta q_i \quad \text{years} \qquad (25)$$

The result of this summation is $t = 5.1 \times 10^9$ years. This is the time it has taken the main sequence to burn down to $M_{Bol} = +3.5$ in M92 and M3 and measures the time since all stars were on the main sequence in these clusters. The agreement of this age with the values currently adopted of 3.55×10^9 years for the age of the crust of the earth and about 4×10^9 years for the age by the expansion constant for extra-galactic nebulae lends credulity to the general features of the evolutionary theory.

It must be stated however that this time computation is quite sensitive to the absolute luminosity, L_i, for stars at the turn off point. If the modulus of M3 were incorrect by say 0.2 magnitudes, the time computed with equation 25 would be incorrect by

about 20 per cent. Thus, within the frame work of this theory we have a new and completely independent method of calibration of the RR Lyrae variables. Suppose we adopt the time of 3.5 for the age of the universe as given by the radioactive age of the earth's crust. If we require the left side of equation 25 to equal this value, the luminosity of the stars at the Schönberg-Chandrasekhar limit would be about 45 per cent higher or $\Delta m = 0.41$. This would require $M_V = +3.1$ for the stars at the turn off and would change the absolute magnitude of all stars by this Δm. The RR Lyrae variables would then be at $M_V = -0.4$. Although it is not suggested that this is a good method for calibration of the cluster variables the example does illustrate how sensitive the time computed by equation 25 is to the absolute magnitude of the cluster variables.

3.3 The Evolutionary Picture for Stars Brighter Than $M_{Bol} = +2$.

Only the lower part of the color-magnitude diagram for globular clusters has been explained in any detail by the models discussed in the previous section. No theoretical models now in existence are adequate to explain the parts of the H-R diagram brighter than

$M_V = +2$. However the general features which a detailed theory of evolution must achieve for these bright type II sequences is rather clear. Speculation concerning the evolution along these sequences is the subject of this section.

Whenever the evolution tracks for stars of different mass are given in the H-R diagram, one can derive a curve crossing the tracks connecting all points reached by stars at the same time. This locus of constant time will be the instantaneous appearance of the H-R diagram for the system. The evolutionary times, computed from the models discussed in section 3.2, are very fast once the star leaves the main sequence. This high rate of evolution requires that the locus of constant time must be very nearly parallel to the evolutionary track of a single star. Hence all stars along this locus must have nearly the same mass. (There must, of course, be a slight difference in mass of the brightest stars compared with those just at the turn-off point; otherwise, all stars in the giant region would be at the same stage of their evolutionary history and the sequences would be populated only in one small region.)

One can therefore conclude that the evolutionary tracks for these bright giant stars, which must eventually be given by detailed model calculations, will be very close to the sequences of Figure 1, Chapter 1.

Stars on the horizontal branch are presumably stars even later in their evolutionary life than those on the giant branch. One is forced to this conclusion by the following argument. These stars, especially those on the blue side of the variable star gap, are once again in the vicinity of the main sequence, from which they originated. Consequently they must again be nearly chemically homogeneous. If this were not so, a mean molecular weight difference between the inner and outer portions of the structure would exist and the star would be in the giant region of the diagram according to the arguments of Öpik [1], and Hoyle and Lyttleton.[2] This means that the stars on the horizontal branch have helium rich cores which have grown to include most of the interior, indicating that these stars are well advanced in their evolution. These stars are moving from right to left on the horizontal sequence as they approach chemical

homogeneity and consequently are quite deficient in hydrogen when they cross the main sequence. Since it seems natural to assume that eventually most of the hydrogen of any star will be used up in models which have gone through most of their evolutionary life, the horizontal branch stars in the vicinity of the main sequence are not unexpected.

If the helium rich core in these stars approaches close to the surface, as it must when the star becomes nearly chemically homogeneous, the hydrogen connective zone might mix appreciable quantities of helium into the atmospheric layers responsible for the formation of spectral lines and thus produce spectra which show hydrogen poor, helium rich characteristics.

Can anything be said of the subsequent history of stars after they have reached this exhausted hydrogen stage? It may be supposed that stars which have consumed most of their hydrogen, decrease in luminosity due to a lack of a suitable fuel and may fall into the white dwarf state. Stars whose masses are greater than the Chandrasekhar limiting mass[6] of $\approx 1.5\ M_{\odot}$ may well become novae in the region $M_V = +3$ to $+6$ at very blue color indices. As novae, they lose mass by

recurrent eruptions until they are below this limit of 1.5 M ⊙. Indeed the very blue sequence populated by 5 stars coming off the end of the horizontal branch in Figure 1, Chapter 1, does seem to be headed for this pre- and post-novae region.

3.4 A Comparison of the Theory with The Observations

Does this suggested evolutionary hypothesis find support from the known facts? There are several predictions from the reasoning of sections 3.2 and 3.3 which can be empirically checked. These are:

(1) All stars brighter than $M_V = +4.5$ should have nearly the same mass and equal to about that of the sun. This implies that the normal mass-luminosity law should not apply to type II stars brighter than $M_V = +4.5$.

(2) The luminosity function $\varphi(M)$ from $M_V = +4.5$ to $\sim +2$ should be that given by a "steady streaming" of stars moving along the sequences of Figure 1, Chapter 1 instead of the primeval luminosity function [presumably the van Rhijn $\varphi(M)$] which is governed by the particular initial conditions at the time of star formation.

(3) The stars along the horizontal branch may show hydrogen poor, helium rich characteristics in their spectra.

The first two predictions seem to be verified from the data in the first two chapters of this thesis while the third prediction agrees with unpublished observations by Greenstein and Münch.

Discussion of all three points follows.

Prediction 1.

There are two ways by which the masses of stars along the subgiant and giant sequences of a globular cluster may be obtained. (1) Binary stars whose orbital elements are known and which populate the same sequences as those of Figure 1, may be used for mass determinations. (2) Dynamical arguments concerning the projected density distribution $\rho(m, r)$ in M3 may give evidence for mass ratios. The first procedure is by far the most reliable since the assumption of statistical equilibrium must be made in method (2) before conclusions from the observed segregation of the bright and faint stars are meaningful. Fortunately, there is one good case of a binary star whose orbital elements are well known which populates the subgiant sequence. This star is ζ Herculis. The most

recent astrometric data for this star are those of R. G. Hall, Jr.[7]. Hall's value for the mass of the brighter component is 1.12 M ⊙. H. L. Johnson's photoelectric data[8] for ζ Herculis gives P - V = +0.53, V = 2.82 which together with Hall's parallax of $\pi = 0''.102 \pm 0''.003$ gives $M_V = 2.86 \pm 0.06$. These data place ζ Herculis precisely on the subgiant sequence of M3 (Figure I). This is excellent evidence that ζ Herculis is analogous to the globular cluster subgiants (or conversely that the zero point of the absolute magnitude scale for M3 is correctly determined as $M_V = 0.0$ for the cluster variables). The mass of 1.12 M ⊙ for the bright component of ζ Her is well determined. This star deviates by 1.2 magnitudes from the mass-luminosity law in the same that it is too bright for its mass. If ζ Herculis is typical of all subgiants, prediction 1 is verified to $M_V = +2.8$. Brighter than $M_V \approx +2.8$ arguments based upon the form of $\rho(m, r)$ in globular clusters must be used to test prediction 1.

If M3 is in statistical equilibrium (i.e. if a Maxwellian velocity distribution obtains) segregation of stars of different masses should occur. If a mass-luminosity law operates for these stars, the form of

$\rho(M, r)$ should depend upon the magnitude, M, of the stars considered. If, however, the masses of the stars are independent of the luminosity from M_i to M_j, $\rho(M, r)$ will not be a function of M in this magnitude interval. The data on $\rho(M, r)$ in Table 10 and Figure 13 of Chapter 2 show that from $M_V = -3$ to $+4$ ($m_{pv} = 12.5$ to 19.5) the function $\rho(m, r)$ is of the type $\rho(m_1, r) = c\ \rho(m_2, r)$ where c is not a function of m. However, fainter than this, segregation takes place so that the form of $\rho(m, r)$ depends upon m. If the age of 5×10^9 years is significantly greater than the relaxation time for M3, the above argument is valid. The fact that no such change in the form of $\rho(m, r)$ is observed until stars of absolute magnitude $+4$ is reached may mean that all stars brighter than this magnitude have the same mass. Although the argument must be viewed with caution, the results of Figure 13 agree with expectations from theory.

Prediction 2.

The luminosity function, $\Phi(M)$, of Table 8 and Figure 10 should give some clue as to the validity of the evolutionary interpretation of the sequences. If the sequences of Figure 1 are a result of the

"steady streaming" of stars in their evolutionary paths, the number of stars per luminosity interval should be proportional to the time spent in that interval. Let X be the hydrogen, Y the helium, and Z the heavy element content by weight of stars. In time δt a star of absolute luminosity L will release $L\delta t$ ergs of radiant energy. If this energy comes from hydrogen conversion into helium,

$$L\delta t \propto dX \tag{26}$$

However from the theory of stellar structure (for stars of the same mass and neglecting a small radius factor)

$$L = A \mu^{7.5} \tag{27}$$

where μ, the mean molecular weight, is given by

$$\mu^{-1} = 2X + \frac{3}{4}Y + \frac{1}{2}Z \tag{28}$$

Hence

$$L \propto \left(2X + \frac{3}{4}Y + \frac{1}{2}Z\right)^{-7.5} \tag{29}$$

Differentiating 29 gives

$$dX \propto \frac{dL}{\mu^{8.5}} \tag{30}$$

Substitution of 30 in 26 and using 27 gives

$$\delta t \propto \frac{dL}{L(\mu)^{8.5}} \propto \frac{dL}{(L)^{32/15}} \tag{31}$$

Hence the time t required for a star to evolve from L_1 to L_2 is

$$t = \text{const} \int_{L_1}^{L_2} \frac{d\,L}{(L)^{32/15}} = \text{const} \left[\left(\frac{1}{L_2} \right)^{17/15} - \left(\frac{1}{L_1} \right)^{17/15} \right] \tag{32}$$

For steady streaming, this time must be proportional to the number of stars between L_1 and L_2. Since the luminosity function is defined as the number of stars between M and M + 0.2, the steady streaming hypothesis requires that

$$\varphi(M_2) \propto t = \frac{\text{const}}{(L_2)^{17/15}} \left[1 - \left(\frac{1}{1.202} \right)^{17/15} \right] =$$

$$= \frac{\text{const}}{(L)^{17/15}} \qquad (33)$$

(since $M_1 = M_2 + 0.2$ or $\frac{L_2}{L_1} = 1.202$)

Furthermore, by definition $M_2 = 2.5 \log \frac{1}{L_2}$ and 33 becomes

$$\log \varphi (M) = \left(\frac{17}{15} \right) \left(\frac{2}{5} \right) M + \text{const}$$

or $$\log \varphi(M) = .454\, M_{Bol} + \text{const} \qquad (34)$$

The relation is expected to hold from the point in the H-R diagram where the evolution begins to the point where equation 27 is no longer valid. Equation 27 is invalid when the models differ greatly from the main sequence models since the eigen value of the problem, which is essentially the parameter A, will depend upon L and R and hence

will no longer be a constant. One should therefore not be surprised if equation 34 fails for bright M_{Bol}. For faint magnitudes equation 34 should be valid to about $M_{Bol} = +4.5$ which is the point one magnitude fainter than the turn off point, and is the place where the evolution is believed to start. Furthermore, equation 34 is valid only if all stars now along the subgiant and transition sequence of Figure 1 originated from a single initial point on the main sequence. If they originated along a small segment of the main sequence, the original $\varphi(M)$ for this segment will be folded into equation 33 causing the number of bright stars to be fewer than equation 34 predicts. A deviation of the data of Table 8 from equation 34 is therefore expected in the sense of having a slightly greater slope. The empirical data of Table 8 give

$$\log \varphi(M) = .380\, M_{Bol} + \text{const} \quad \left[+0.7 < M_{Bol} < +4.0\right] \tag{35}$$

This is so close to equation 34 when the correction due to the finite width of the region of origin is considered that the requirement for the sequences of Figure 1 to be evolutionary is considered

likely. Furthermore the limit of validity of equation 35 at the faint end shows that the evolution starts at about $M_{Bol} \approx +4$. This is only slightly brighter than the one magnitude below the Schönberg-Chandrasekhar limiting configuration required by theory.

Prediction 3.

The third prediction from the evolutionary hypothesis concerns the hydrogen content of the stars on the horizontal branch. Recent unpublished spectral observations by Greenstein of the Humason-Zwicky stars near the galactic pole and by Münch of the M3 stars on the horizontal branch show that these stars have pronounced hydrogen poor, helium rich characteristics. Prediction 3 seems therefore to be confirmed.

All data now available thus lend support to an evolutionary explanation of the sequences in the color-magnitude diagrams of globular clusters. It remains however to produce evolutionary stellar models which will explain all details of Figure 1 and make the hypothesis advanced in this chapter more than speculation.

References for Chapter 3

1. E. J. Öpik, Tartu Obs. Pub., 30, Nos. 3 and 4, 1938

2. F. Hoyle and R. A. Lyttleton, M.N., 102, 218, 1942

3. B. Strömgren, A.J., 57, 65, 1952

4. A. R. Sandage and M. Schwarzschild, Ap.J., 116, 463, 1952

5. Schönberg and Chandrasekhar, Ap.J., 96, 161, 1942

6. S. Chandrasekhar, Stellar Structure, Chapter 11, University of Chicago Press

7. R. G. Hall, Jr., A.J., 54, 199, 1948

8. H. L. Johnson, Unpublished data kindly made available.